median time from transplantation to the onset of cGVHD in patients with overlap syndrome was shorter compared to patients with classic cGVHD (4.1 vs. 7.1 months, $P < 0.001$). All patients with overlap syndrome were graded as having moderate or severe cGVHD, whereas the proportion of patients who developed severe cGVHD was similar between patients with classic cGVHD and those with overlap syndrome. Proportions of patients with platelet counts less than $100 \times 10^3/\mu L$, eosinophil counts less than $500/\mu L$, and ongoing systemic corticosteroid treatment at the onset of cGVHD were higher among patients who developed overlap syndrome compared with those who developed classic cGVHD.

3.2 Chronic GVHD-specific survival

Of the 96 patients who developed NIH cGVHD, recurrent or secondary malignant neoplasm occurred in 27 patients and death due to any cause occurred in 31 patients. The respective 3-year probabilities of cGSS among patients who developed classic cGVHD and overlap syndrome were 88 and 70% ($P = 0.060$) (Fig. 1a), while those among subgroups of patients graded to have mild, moderate, and severe cGVHD at onset were 100, 86, and 69% (mild to moderate vs. severe, $P = 0.034$) (Fig. 1b). Table 3 shows the results of univariable and multivariable analyses for factors potentially associated with cGSS among the patients who developed NIH cGVHD. In univariable analysis, the presence of severe cGVHD and thrombocytopenia at cGVHD onset were significantly associated with lower cGSS, whereas the presence of an overlap syndrome and high-risk malignant disease tended to be associated with lower cGSS. In multivariable analysis, the presence of thrombocytopenia at cGVHD onset was the only significant factor that adversely affected cGSS [hazard ratio (HR) for mortality = 4.05, 95% confidence interval (CI) = 1.35–12.1, $P = 0.013$], although patients with severe cGVHD (HR = 2.58, 95% CI = 0.90–7.39, $P = 0.077$) or those with high-risk underlying disease (HR = 2.75, 95% CI = 0.86–8.80, $P = 0.088$) also had a trend toward lower cGSS.

3.3 Duration of systemic immunosuppressive treatment

A total of 81 patients received systemic immunosuppressive agents for the treatment of NIH cGVHD. In this group of patients, the cumulative incidence of withdrawal of systemic IST was 40% (95% CI = 29–51%) at 3 years after the onset of cGVHD, while the cumulative incidence of the competing risks of death or recurrent/secondary malignancy during systemic IST was 42% (95% CI = 32–55%) (Fig. 2). In univariable analysis, no significant association was found between discontinuation of IST and subcategory or global severity of NIH cGVHD (overlap syndrome vs. classic cGVHD, HR for IST withdrawal = 0.51, 95% CI = 0.20–1.31, $P = 0.16$; severe vs. mild to moderate, HR = 0.90, 95% CI = 0.42–1.96, $P = 0.80$). Multivariable analysis revealed two factors significantly associated with prolonged administration of systemic IST; high-risk primary disease (HR = 0.39, 95% CI = 0.19–0.77, $P = 0.007$) and the ongoing use of systemic corticosteroids at the onset of cGVHD (HR = 0.40, 95% CI = 0.19–0.84, $P = 0.015$).

3.4 Non-relapse mortality

Death from non-relapse causes occurred in 16 (17%) of 96 patients who developed NIH cGVHD and in 10 (9%) of 115 patients who did not. In a multivariable analysis of the entire series of 211 patients, treating the subcategory or peak severity of NIH cGVHD as a time-dependent covariate, development of the overlap syndrome or severe cGVHD was significantly associated with higher risk of NRM compared to the absence of cGVHD (overlap syndrome vs. no cGVHD, HR = 3.90, 95% CI = 1.32–11.6, $P = 0.014$; severe cGVHD vs. no cGVHD, HR = 6.21, 95% CI = 2.25–17.1, $P < 0.001$). Development of classic cGVHD or mild-to-moderate cGVHD was not significantly associated with higher risk of NRM when compared with the absence of NIH cGVHD (classic cGVHD vs. no cGVHD, HR for mortality = 1.39, 95% CI = 0.55–3.53, $P = 0.49$; mild-to-moderate cGVHD vs. no cGVHD, HR = 2.25, 95% CI = 0.62–8.18, $P = 0.22$).

4 Discussion

In the present study, we evaluated the clinical significance of subcategory and severity of NIH cGVHD in terms of their influences on cGSS, discontinuation of IST, and NRM using a retrospective cohort of patients who underwent allo-HCT for hematologic disorders. In univariable analysis, patients with overlap syndrome tended to have a lower probability of cGSS than those with classic cGVHD, while patients who developed severe cGVHD had significantly worse cGSS compared with those who developed mild-to-moderate cGVHD. Although such differences in cGSS according to NIH cGVHD subtypes did not reach statistical significance by multivariable analysis, patients who developed overlap syndrome or severe NIH cGVHD had a significantly higher NRM than those who did not develop any manifestation of NIH cGVHD. These results suggest that both subcategory and global severity of NIH cGVHD might be useful for evaluating the risk of GVHD-associated mortality in patients diagnosed to have cGVHD by the NIH criteria. In

Table 2 Characteristics of chronic GVHD according to subcategory defined by the National Institutes of Health criteria

Characteristics	Total ($n = 96$)	NIH cGVHD subcategory		
		Classic cGVHD ($n = 77$)	Overlap syndrome ($n = 19$)	P value
Median months (range) to onset of cGVHD	6.7 (2.1–29.9)	7.1 (2.7–29.9)	4.1 (2.1–20.7)	<0.001
Involved organs or sites[a], n (%)[b]				0.92
Skin	55 (57)	40 (52)	15 (79)	
Mouth	69 (72)	56 (73)	13 (68)	
Eyes	29 (30)	23 (30)	6 (32)	
Gastrointestinal tract	34 (35)	25 (32)	9 (47)	
Liver	76 (79)	61 (79)	15 (79)	
Lungs	12 (12)	9 (12)	3 (16)	
Joints and fascia	4 (4)	3 (4)	1 (5)	
Genital tract	2 (2)	2 (3)	0 (0)	
Number of involved organs or sites[a], n (%)				0.14
1	7 (7)	7 (9)	0 (0)	
2	27 (28)	24 (31)	3 (16)	
3 or more	62 (65)	46 (60)	16 (84)	
Maximum score of involved organs[a], n (%)				0.18
Score 1	22 (23)	20 (26)	2 (11)	
Score 2 (other than lungs)	26 (27)	18 (62)	8 (42)	
Score 2 (lungs)	6 (6)	4 (5)	2 (11)	
Score 3	42 (44)	35 (45)	7 (37)	
Severity at onset, n (%)				0.023
Mild	20 (21)	20 (26)	0 (0)	
Moderate	53 (55)	39 (51)	14 (74)	
Severe	23 (24)	18 (23)	5 (26)	
Severity at peak, n (%)				0.17
Mild	12 (13)	12 (16)	0 (0)	
Moderate	39 (41)	29 (38)	10 (53)	
Severe	45 (47)	36 (47)	9 (47)	
Platelet count at cGVHD onset, n (%)				0.002
$100 \times 10^3/\mu L$ or more	65 (68)	58 (75)	7 (37)	
Less than $100 \times 10^3/\mu L$	31 (32)	19 (25)	12 (63)	
Eosinophil count at cGVHD onset, n (%)				0.010
Less than 500/μL	68 (71)	50 (65)	18 (95)	
500/μL or more	28 (29)	27 (35)	1 (5)	
Systemic corticosteroids at cGVHD onset, n (%)				<0.001
Not received	63 (66)	61 (79)	2 (11)	
Received	33 (34)	16 (21)	17 (89)	

cGVHD chronic graft-versus-host disease

[a] Data evaluated at peak clinical worsening are shown

[b] The sum of the number per involved site is not equal to the number of evaluable patients, because the involvement of more than one organ can occur in a single patient. Accordingly, the sum of percentage among the total number of patients does not equal to one hundred

contrast, duration of IST was neither affected by NIH cGVHD subcategory nor by its severity.

While cGSS has been frequently used as a study endpoint to describe the mortality attributable to cGVHD-associated organ dysfunction, there have been no established early surrogates that help to guide the clinical management of patients with evidence of ongoing cGVHD. Given that the historic limited/extensive grading system is not a useful predictor for the severity of organ involvement in terms of mortality risk, several studies have attempted to develop

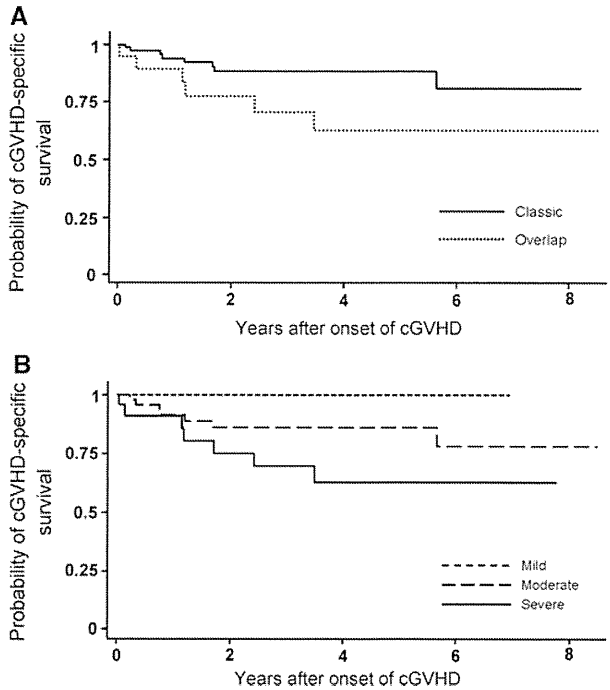

Fig. 1 Chronic GVHD-specific survival in patients with chronic GVHD diagnosed by the NIH consensus criteria. **a** Probability of chronic GVHD-specific survival (cGSS) among patients who developed classic chronic GVHD (*solid line*) and overlap syndrome (*dotted line*). **b** Probability of cGSS among patients who developed mild (*short dashed line*), moderate (*long dashed line*), and severe chronic GVHD (*solid line*)

improved grading scales for established cGVHD. A retrospective analysis of data on HLA-identical sibling transplantation reported to the International Bone Marrow Transplant Registry identified five variables independently associated with worse survival of those who developed historic cGVHD: low Karnofsky performance status at cGVHD diagnosis (<80), chronic diarrhea, weight loss, presence of cutaneous manifestation, and lack of oral involvement [15]. The Seattle group also proposed a revised classification for distinguishing limited and extensive cGVHD by the use of 16 clinical criteria [16]. Although these new classifications do not clearly discriminate between cGVHD and delayed onset GVHD with features resembling aGVHD, they have been shown to be at least useful for identifying patients at higher risk of NRM. Future studies are strongly warranted to compare the prognostic values of NIH cGVHD subcategories with those determined by other cGVHD grading system [21].

So far, several groups have reported the prognostic relevance of cGVHD severity graded by the NIH criteria and consistently found the inferior survival of patients with severe cGVHD [20–23], although such association was not observed in one earlier study [19]. While only a few of these studies focused on the significance of distinction between "overlap syndrome" and "classic cGVHD", our study revealed a trend toward worse survival in patients with overlap syndrome compared to those with classic GVHD, as was recently reported by Kim et al. [23]. In the present study, patients with overlap syndrome had a significantly shorter median time to the development of cGVHD than patients with classic cGVHD and were more likely to receive corticosteroid treatment for prior aGVHD at the onset of cGVHD. Intriguingly, these observations were very similar to the findings by Arora et al. [22], who reported that most of patients with overlap syndrome had a history of prior aGVHD and a progressive cGVHD onset, although they did not observe worse survival of this subgroup of patients compared to those with classic cGVHD. Given that nearly all patients who developed overlap syndrome had a prior history of aGVHD in our study cohort, NIH overlap syndrome in most instances could be considered as a flare of preexisting aGVHD, concomitant with development of classic cGVHD. In this context, it is important to note that early flare of cGVHD or early treatment change for exacerbation of cGVHD has been reported to be associated with increased NRM and inferior cGSS [34, 35]. It is also of note that a significantly higher proportion of patients with overlap syndrome had thrombocytopenia less than $100 \times 10^3/\mu L$ at cGVHD onset in our study. Since the progressive cGVHD onset and the presence of thrombocytopenia were consistently associated with an increased NRM across various studies [16, 36], more effective management of patients with overlap syndrome and thrombocytopenia might be needed.

Duration of systemic immunosuppressive therapy is suggested to be a useful surrogate endpoint to evaluate the response to specific treatment for cGVHD [26]. Although we could not find significant association of NIH cGVHD subtypes with duration of systemic IST, patients who had been given ongoing systemic corticosteroids at the onset of cGVHD were found to receive significantly prolonged systemic IST in multivariable analysis, consistent with the findings of Vigorito et al. [37]. In our study, the duration of systemic IST was also prolonged in patients who had high-risk underlying disease compared with those who had standard-risk disease. If the activity of cGVHD were likely to worsen in the high-risk subgroup of patients, one possible explanation might be the preference of physicians to taper systemic IST faster for patients at higher risk of relapse.

The present study, however, has several limitations; the retrospective study design, small cohort size, recording bias, and heterogeneity of underlying diseases and transplantation procedures might substantially influence the results. In addition, diagnostic cGVHD manifestations of affected organs or sites might have originated from other causes, including drug reactions, infection, and

Table 3 Univariable and multivariable analysis of factors potentially associated with chronic GVHD-specific survival among patients who developed chronic GVHD defined by the National Institutes of Health criteria

Variable	*n* (%)	Univariable analysis		Multivariable analysis	
		HR (95% CI)	*P* value	HR (95% CI)	*P* value
Patient age					
Less than 50 years	51 (53)	1.00		–	
50 years or more	45 (47)	1.40 (0.49–4.05)	0.53	–	
Donor/recipient sex combination					
Other than female/male	69 (72)	1.00		–	
Female/male	27 (28)	1.03 (0.32–3.28)	0.97	–	
Disease status at transplant					
Standard risk	51 (53)	1.00		1.00	
High risk	45 (47)	3.03 (0.95–9.68)	0.061	2.75 (0.86–8.80)	0.088
Donor/recipient HLA compatibility					
Matched	80 (83)	1.00		–	
Mismatched	16 (17)	0.33 (0.04–2.53)	0.29	–	
Conditioning regimen					
Myeloablative intensity	54 (56)	1.00		–	
Reduced intensity	42 (44)	1.04 (0.36–3.00)	0.95	–	
Stem cell source					
Bone marrow	67 (70)	1.00		–	
Peripheral blood	24 (25)	2.07 (0.69–6.19)	0.19	–	
Cord blood	5 (5)	1.63 (0.57–4.68)	0.37	–	
Prior aGVHD					
Grade 0–1	47 (49)	1.00		–	
Grade 2–4	49 (51)	1.16 (0.40–3.37)	0.78	–	
Subcategory of cGVHD					
Classic cGVHD	77 (80)	1.00		–	
Overlap syndrome	19 (20)	2.76 (0.96–7.97)	0.060	–	
Severity of cGVHD at onset					
Mild to moderate	73 (76)	1.00		1.00	
Severe	23 (24)	3.10 (1.09–8.86)	0.034	2.58 (0.90–7.39)	0.077
Platelet count at cGVHD onset					
$100 \times 10^3/\mu L$ or more	65 (68)	1.00		1.00	
Less than $100 \times 10^3/\mu L$	31 (32)	4.19 (1.40–12.5)	0.010	4.05 (1.35–12.1)	0.013
Eosinophil count at cGVHD onset					
Less than 500/μL	68 (71)	1.00		–	
500/μL or more	28 (29)	0.90 (0.28–2.88)	0.86	–	
Systemic corticosteroids at cGVHD onset					
Not received	63 (66)	1.00		–	
Received	33 (34)	1.74 (0.61–4.97)	0.30	–	

CI confidence interval, *aGVHD* acute graft-versus-host disease, *cGVHD* chronic graft-versus-host disease

comorbidity before transplantation. Furthermore, genital tract involvement might be underestimated because female patients do not always report about their genital symptoms to physicians.

In conclusion, our present study suggests that both the subcategory and global severity of cGVHD proposed by NIH consensus criteria have effects on cGSS and the risk of NRM among patients who develop NIH cGVHD. Future prospective studies are warranted to more precisely characterize the clinical significance of the subcategory and severity of cGVHD evaluated by the NIH consensus criteria.

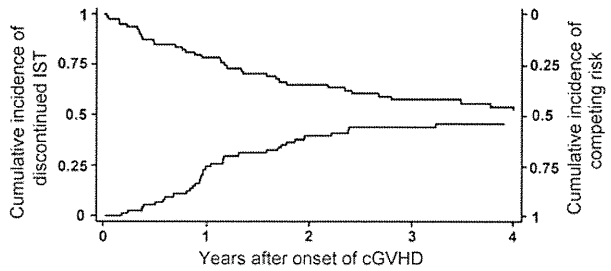

Fig. 2 Cumulative incidence of discontinued systemic immunosuppressive treatment. The *lower curve* shows the cumulative incidence of discontinued systemic immunosuppressive treatment (IST) in the absence of death, recurrent primary disease, or secondary malignancy among 81 patients who developed NIH cGVHD and received systemic IST (*left-hand scale*). The *upper curve* shows the competing risks of death or recurrent/secondary malignancy during systemic IST (*right-hand scale*). At the onset of cGVHD, 69 patients had been already given ongoing systemic IST consisting of calcineurin inhibitors alone ($n = 36$), calcineurin inhibitors plus corticosteroids ($n = 27$), corticosteroids alone ($n = 4$), or corticosteroids plus mycophenolate mofetil ($n = 2$)

Acknowledgments The authors are grateful to Rie Goi and Mika Kobayashi, for their expert data management and secretarial assistance, and all the staff of our transplant team for their dedicated care of the patients and donors.

Conflict of interest The authors have no conflict of interest to declare.

References

1. Lee S, Flowers M. Recognizing and managing chronic graft-versus-host disease. Hematology Am Soc Hematol Educ Program. 2008:134–41.
2. Atkinson K, Horowitz M, Gale R, et al. Risk factors for chronic graft-versus-host disease after HLA-identical sibling bone marrow transplantation. Blood. 1990;75:2459–64.
3. Higman M, Vogelsang G. Chronic graft versus host disease. Br J Haematol. 2004;125:435–54.
4. Wagner J, Flowers M, Longton G, Storb R, Schubert M, Sullivan K. The development of chronic graft-versus-host disease: an analysis of screening studies and the impact of corticosteroid use at 100 days after transplantation. Bone Marrow Transplant. 1998;22:139–46.
5. Przepiorka D, Anderlini P, Saliba R, et al. Chronic graft-versus-host disease after allogeneic blood stem cell transplantation. Blood. 2001;98:1695–700.
6. Carlens S, Ringdén O, Remberger M, et al. Risk factors for chronic graft-versus-host disease after bone marrow transplantation: a retrospective single centre analysis. Bone Marrow Transplant. 1998;22:755–61.
7. Cutler C, Giri S, Jeyapalan S, Paniagua D, Viswanathan A, Antin J. Acute and chronic graft-versus-host disease after allogeneic peripheral-blood stem-cell and bone marrow transplantation: a meta-analysis. J Clin Oncol. 2001;19:3685–91.
8. Mohty M, Kuentz M, Michallet M, et al. Chronic graft-versus-host disease after allogeneic blood stem cell transplantation: long-term results of a randomized study. Blood. 2002;100:3128–34.
9. Randolph S, Gooley T, Warren E, Appelbaum F, Riddell S. Female donors contribute to a selective graft-versus-leukemia effect in male recipients of HLA-matched, related hematopoietic stem cell transplants. Blood. 2004;103:347–52.
10. Atsuta Y, Suzuki R, Yamamoto K, et al. Risk and prognostic factors for Japanese patients with chronic graft-versus-host disease after bone marrow transplantation. Bone Marrow Transplant. 2006;37:289–96.
11. McClune B, Weisdorf D, Pedersen T, et al. Effect of age on outcome of reduced-intensity hematopoietic cell transplantation for older patients with acute myeloid leukemia in first complete remission or with myelodysplastic syndrome. J Clin Oncol. 2010;28:1878–87.
12. Mielcarek M, Martin P, Leisenring W, et al. Graft-versus-host disease after nonmyeloablative versus conventional hematopoietic stem cell transplantation. Blood. 2003;102:756–62.
13. Mielcarek M, Burroughs L, Leisenring W, et al. Prognostic relevance of 'early-onset' graft-versus-host disease following nonmyeloablative haematopoietic cell transplantation. Br J Haematol. 2005;129:381–91.
14. Shulman H, Sullivan K, Weiden P, et al. Chronic graft-versus-host syndrome in man. A long-term clinicopathologic study of 20 Seattle patients. Am J Med. 1980;69:204–17.
15. Lee S, Klein J, Barrett A, et al. Severity of chronic graft-versus-host disease: association with treatment-related mortality and relapse. Blood. 2002;100:406–14.
16. Lee SJ, Vogelsang G, Flowers MED. Chronic graft-versus-host disease. Biol Blood Marrow Transplant. 2003;9:215–33.
17. Atkinson K, Horowitz M, Gale R, Lee M, Rimm A, Bortin M. Consensus among bone marrow transplanters for diagnosis, grading and treatment of chronic graft-versus-host disease. Committee of the International Bone Marrow Transplant Registry. Bone Marrow Transplant. 1989;4:247–54.
18. Filipovich AH, Weisdorf D, Pavletic S, et al. National Institutes of Health consensus development project on criteria for clinical trials in chronic graft-versus-host disease: I. Diagnosis and staging working group report. Biol Blood Marrow Transplant. 2005;11:945–56.
19. Jagasia M, Giglia J, Chinratanalab W, et al. Incidence and outcome of chronic graft-versus-host disease using National Institutes of Health consensus criteria. Biol Blood Marrow Transplant. 2007;13:1207–15.
20. Pérez-Simón J, Encinas C, Silva F, et al. Prognostic factors of chronic graft-versus-host disease following allogeneic peripheral blood stem cell transplantation: the National Institutes Health scale plus the type of onset can predict survival rates and the duration of immunosuppressive therapy. Biol Blood Marrow Transplant. 2008;14:1163–71.
21. Cho B, Min C, Eom K, et al. Feasibility of NIH consensus criteria for chronic graft-versus-host disease. Leukemia. 2009;23:78–84.
22. Arora M, Nagaraj S, Witte J, et al. New classification of chronic GVHD: added clarity from the consensus diagnoses. Bone Marrow Transplant. 2009;43:149–53.
23. Kim D, Lee J, Kim S, et al. Reevaluation of the National Institutes of Health criteria for classification and scoring of chronic GVHD. Bone Marrow Transplant. 2010;45:1174–80.
24. Flowers MED, Parker PM, Johnston LJ, et al. Comparison of chronic graft-versus-host disease after transplantation of peripheral blood stem cells versus bone marrow in allogeneic recipients: long-term follow-up of a randomized trial. Blood. 2002; 100:415–9.
25. Stewart B, Storer B, Storek J, et al. Duration of immunosuppressive treatment for chronic graft-versus-host disease. Blood. 2004;104:3501–6.
26. Martin P, Weisdorf D, Przepiorka D, et al. National Institutes of Health Consensus Development Project on Criteria for clinical

trials in chronic graft-versus-host disease: VI. Design of Clinical Trials Working Group report. Biol Blood Marrow Transplant. 2006;12:491–505.
27. Kitawaki T, Kadowaki N, Ishikawa T, Ichinohe T, Uchiyama T. Compromised recovery of natural interferon-alpha/beta-producing cells after allogeneic hematopoietic stem cell transplantation complicated by acute graft-versus-host disease and glucocorticoid administration. Bone Marrow Transplant. 2003;32:187–94.
28. Mizumoto C, Kanda J, Ichinohe T, et al. Mycophenolate mofetil combined with tacrolimus and minidose methotrexate after unrelated donor bone marrow transplantation with reduced-intensity conditioning. Int J Hematol. 2009;89:538–45.
29. Kanda J, Mizumoto C, Kawabata H, et al. Clinical significance of serum hepcidin levels on early infectious complications in allogeneic hematopoietic stem cell transplantation. Biol Blood Marrow Transplant. 2009;15:956–62.
30. Przepiorka D, Weisdorf D, Martin P, et al. 1994 Consensus Conference on acute GVHD grading. Bone Marrow Transplant. 1995;15:825–8.
31. Gooley TA, Leisenring W, Crowley J, Storer BE. Estimation of failure probabilities in the presence of competing risks: new representations of old estimators. Stat Med. 1999;18:695–706.
32. Kim H. Cumulative incidence in competing risks data and competing risks regression analysis. Clin Cancer Res. 2007; 13:559–65.
33. Cortese G, Andersen P. Competing risks and time-dependent covariates. Biom J. 2010;52:138–58.
34. Kim DH, Sohn SK, Baek JH, et al. Time to first flare-up episode of GVHD can stratify patients according to their prognosis during clinical course of progressive- or quiescent-type chronic GVHD. Bone Marrow Transplant. 2007;40:779–84.
35. Flowers MED, Storer B, Carpenter P, et al. Treatment change as a predictor of outcome among patients with classic chronic graft-versus-host disease. Biol Blood Marrow Transplant. 2008;14:1380–4.
36. Akpek G, Zahurak M, Piantadosi S, et al. Development of a prognostic model for grading chronic graft-versus-host disease. Blood. 2001;97:1219–26.
37. Vigorito A, Campregher P, Storer B, et al. Evaluation of NIH consensus criteria for classification of late acute and chronic GVHD. Blood. 2009;114:702–8.

Biochemical and Biophysical Research Communications 413 (2011) 75–79

Contents lists available at SciVerse ScienceDirect

Biochemical and Biophysical Research Communications

journal homepage: www.elsevier.com/locate/ybbrc

Singlet oxygen is essential for neutrophil extracellular trap formation

Yoko Nishinaka [a], Toshiyuki Arai [b], Souichi Adachi [a], Akifumi Takaori-Kondo [c], Kouhei Yamashita [c,*]

[a] School of Human Health Science, Faculty of Medicine, Kyoto University, Kyoto 606-8507, Japan
[b] Department of Anesthesia, Kyoto University Hospital, Kyoto 606-8507, Japan
[c] Department of Hematology and Oncology, Graduate School of Medicine, Kyoto University, Kyoto 606-8507, Japan

ARTICLE INFO

Article history:
Received 10 August 2011
Available online 24 August 2011

Keywords:
Neutrophil extracellular traps (NETs)
Reactive oxygen species (ROS)
Singlet oxygen ($^1O_2$)
NADPH oxidase (Nox)
Chronic granulomatous disease (CGD)
Porfimer sodium (Photofrin)

ABSTRACT

Neutrophil extracellular traps (NETs) that bind invading microbes are pivotal for innate host defense. There is a growing body of evidence for the significance of NETs in the pathogenesis of infectious and inflammatory diseases, but the mechanism of NET formation remains unclear. Previous observation in neutrophils of chronic granulomatous disease (CGD) patients, which defect NADPH oxidase (Nox) and fail to produce reactive oxygen species (ROS), revealed that ROS contributed to the formation of NETs. However, the active species were not identified. In this study, we discovered that singlet oxygen, one of the ROS, mediated Nox-dependent NET formation upon stimulation with phorbol myristate acetate. We also revealed that singlet oxygen itself could induce NET formation by a distinct system generating singlet oxygen with porfimer sodium (Photofrin) in CGD neutrophils, as well as healthy neutrophils. This was independent of Nox activation. These results show that singlet oxygen is essential for NET formation, and provide novel insights into the pathogenesis of infectious and inflammatory diseases.

1. Introduction

Recent investigations highlighted a novel killing mechanism of neutrophils, called neutrophil extracellular traps (NETs), which capture microbes in extracellular structures consisting of DNA fibers and antimicrobial granule proteins [1,2]. There have been many reports on the antimicrobial effects and pro-inflammatory roles of NETs [3], but the mechanism of NET formation remains unclear. Previous observation revealed that reactive oxygen species (ROS) generated by activated neutrophils contributed to the formation of NETs [4]. However, the active species have not been identified.

Neutrophils first generate superoxide anion ($O_2^{\cdot -}$) by NADPH oxidase (Nox) activation, and this $O_2^{\cdot -}$ is converted to hydrogen peroxide (H_2O_2) by superoxide dismutase. Hypochlorous acid (HOCl) is produced from H_2O_2 by myeloperoxidase (MPO), and reacts with H_2O_2 to form singlet oxygen ($^1O_2$) [5]. The role of $^1O_2$ in microbicidal activity is not fully understood. It was recently reported that the ROS with chemical signature of ozone, which is converted from $^1O_2$ by immunoglobulin or several amino acids, contributes to killing of bacteria [6,7]. A recent study showed that MPO is required for NET formation [8], indicative of the involvement of $^1O_2$ in NET formation.

We previously showed that edaravone, (3-methyl-1-phenyl-2-pyrazolin-5-one), a free radical scavenger, and α-phenyl-*N*-*tert*-butyl nitrone (PBN), a spin trap agent, suppressed $^1O_2$ release from activated neutrophils, but did not affect $O_2^{\cdot -}$ release [9,10]. Furthermore, we demonstrated that PBN neither affects MPO activity, nor reacts with HOCl [10].

In this study, we first examined the effect of edaravone or PBN on Nox-dependent NET formation by phorbol myristate acetate (PMA) stimulation, to elucidate the involvement of $^1O_2$ in NET formation. We next studied whether NETs are formed by a distinct system generating $^1O_2$ with porfimer sodium (Photofrin) in neutrophils of a patient with chronic granulomatous disease (CGD), which is an inherited immunodeficiency with Nox defect, leading to recurrent life-threatening infections. These results should uncover an essential role of $^1O_2$ in NET formation.

2. Materials and methods

2.1. Reagents

Hanks' balanced salt solution (HBSS) was purchased from Invitrogen (Carlsbad, CA); trans-1-(2′-methoxyvinyl)pyrene (MVP) and Sytox green were from Molecular Probes (Eugene, OR); and 2-methyl-6-phenyl-3,7-dihydroimidazo[1,2-α]pyrazin-3-one (CLA) was from Tokyo Kasei Kogyo (Tokyo, Japan). PBN was obtained from Radical Research Ltd. (Hino, Tokyo, Japan) and dissolved in phosphate-buffered saline (PBS) to a final concentration 100 mM (pH 7.4). Edaravone was a kind gift from Tanabe–Mitsubishi

* Corresponding author. Address: Department of Hematology and Oncology, Graduate School of Medicine, Kyoto University, 54 Shogoin Kawahara-cho, Sakyo-ku, Kyoto 606-8507, Japan. Fax: +81 75 751 4963.
E-mail address: kouhei@kuhp.kyoto-u.ac.jp (K. Yamashita).

0006-291X/$ - see front matter © 2011 Elsevier Inc. All rights reserved.
doi:10.1016/j.bbrc.2011.08.052

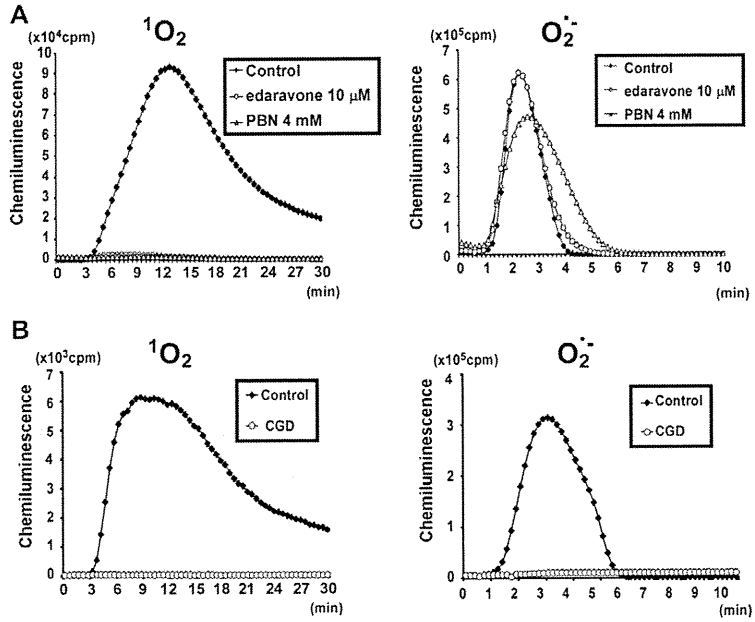

Fig. 1. ROS generation by PMA stimulation. (A) The effect of edaravone or PBN on PMA-stimulated ROS release of healthy neutrophils. ROS generation was examined by chemiluminescence using $^1O_2$- and $O_2^{\cdot-}$-specific probes, MVP (left panel) and CLA (right panel) respectively. Healthy neutrophils (2×10^6 cells) by PMA stimulation (100 ng/ml) with 40 μM MVP (left panel) or 2.5 μM CLA (right panel) in the treatment of 10 μM edaravone or 4 mM PBN mounted on a luminescence reader. The luminescence of MVP or CLA was monitored every 30 s for 30 min or every 10 s for 10 min, respectively. The inhibitory effect on $^1O_2$-release of edaravone or PBN was observed. In contrast, edaravone or PBN did not exhibit the inhibitory effect on $O_2^{\cdot-}$ release. The experiments were performed at least 3 times, and representative data are shown. (B) ROS generation in neutrophils of a healthy volunteer (control) and a CGD patient (CGD). Healthy or CGD neutrophils (2×10^6 cells) by PMA stimulation (100 ng/ml) with 40 μM MVP (left panel) or 2.5 μM CLA (right panel) mounted on a luminescence reader. CGD neutrophils did not produce $^1O_2$- and $O_2^{\cdot-}$.

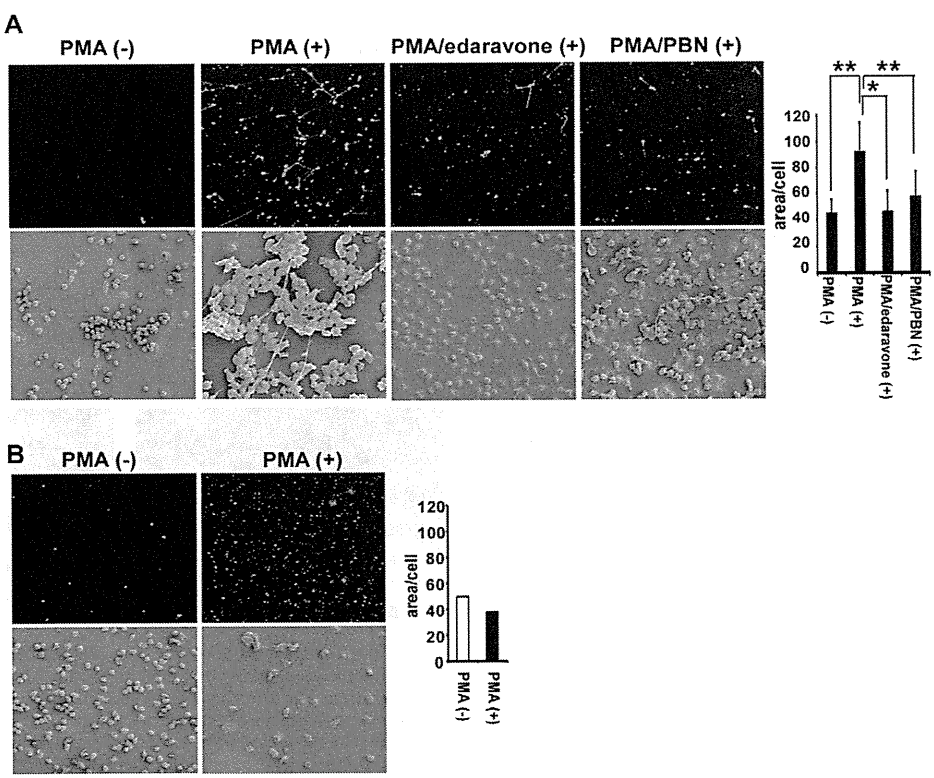

Fig. 2. NET formation by PMA stimulation. (A) NET formation upon stimulation with PMA by fluorescence confocal microscopy and scanning electron microscopy (SEM). Healthy neutrophils stained with 500 nM Sytox green were observed after 3 h of stimulation with PMA (100 ng/ml) by laser-scanning confocal microscopy (upper panels, 100×) and SEM (lower panels, 250×). Representative data are shown. Quantitative analysis was performed using ImageJ software (right graph). The inhibitory effect of edaravone (10 μM) or PBN (4 mM) on PMA-stimulated NET formation was observed. Values are the means ± SD ($n = 5$). * and ** indicate $P < 0.05$ and $P < 0.01$, respectively. (B) NET formation of CGD neutrophils by PMA stimulation by fluorescence confocal microscopy (upper panels, 100×) and SEM (lower panels, 250×). Quantitative analysis was also performed (right graph). Note that NET formation was not observed in a CGD patient.

Pharma Corporation (Tokyo, Japan) and directly dissolved in PBS or D_2O to a final concentration of 4 mM (pH 7.4). Porfimer sodium (Photofrin) was obtained from Pfizer Japan Inc. (Tokyo, Japan). Other chemicals, such as phorbol myristate acetate (PMA), were purchased from Sigma Chemicals (St. Louis, MO).

2.2. Preparation of neutrophils

Human neutrophils were isolated from peripheral blood by sedimentation through two-step Percoll (GE Healthcare Japan, Tokyo, Japan) gradients. The CGD patient was a 24-year-old male with *gp91-phox* deficiency with a G-to-A point mutation at nucleotide 389 in exon 10. Healthy volunteers and the patient provided written informed consent for participation in an institutional review board-approved protocol at Kyoto University Hospital.

2.3. Chemiluminescence assay

The productions of $^1O_2$ and $O_2^{\cdot-}$ of neutrophils stimulated with 100 ng/ml PMA were examined by chemiluminescence using $^1O_2$- and $O_2^{\cdot-}$-specific probes, MVP [11] and CLA [12], respectively. The effect of edaravone and PBN on ROS production was examined. Healthy or CGD neutrophils (2×10^6 cells) were mounted on a luminescence reader (Aloka BLR-310; Aloka, Tokyo, Japan) in the presence of 40 μM MVP or 2.5 μM CLA. After the start of measurement, neutrophils were stimulated with 100 ng/ml PMA. The luminescence of MVP was monitored every 30 s for 30 min and that of CLA was monitored every 10 s for 10 min.

2.4. Analysis of NET formation by PMA stimulation

NET formation was visualized with a laser-scanning fluorescence confocal microscope (Nikon Digital Eclipse C1, Tokyo, Japan) after stimulation of 2×10^6 neutrophils for 3 h with 100 ng/ml PMA and staining of the NET DNA with 500 nM Sytox green. Quantitative analysis was performed using ImageJ software. Briefly, the Sytox-positive area of each micrograph was measured and divided by the total number of Sytox-positive cells, which showed the mean size of nuclear area per cell, whereby a large mean size was suggestive of NETs. NET formation was also visualized with a Hitachi S-4700 scanning electron microscope.

2.5. Detection of $^1O_2$ in a cell-free system

The direct analysis of near-infrared luminescence was performed in a cell-free system using Raman spectroscopy (LabRAM HR-800, HORIBA, Kyoto, Japan), to detect the $^1O_2$ generation by irradiation of porfimer sodium (Photofrin) solution. D_2O was used as the solvent since the lifetime of $^1O_2$ is much longer (62 μs in D_2O than in H_2O (3.8 μs). The quantum yields of $^1O_2$ production were determined by measurement of the $^1O_2$ luminescence at 1270 nm, which originated from continuous irradiation of 100 μg/ml Photofrin solutions using a laser beam (wavelength 632.8 nm, power 6 mW). The luminescence of $^1O_2$ was measured with a liquid nitrogen-cooled InGaAs photodiode in conjunction with a 1270 nm interference filter.

2.6. Analysis of accumulation of Photofrin in neutrophils

Neutrophils (2×10^7/ml) were visualized by fluorescence microscopy using Cy5 filter (Nikon) after incubation with 10 μg/ml Photofrin for 1 h.

2.7. Analysis of NET formation by photochemically generated $^1O_2$

NET formation was analyzed by fluorescence confocal microscopy and scanning electron microscopy (SEM). Neutrophils (2×10^7/ml) were incubated for 1 h after cells were treated with 10 μg/ml Photofrin for 1 h and subjected to irradiation for 5 min using an LED lamp (λ_{max} = 660 nm, CCS Inc., Kyoto, Japan).

2.8. Statistical analysis

Data are expressed as the mean ± SD. $P < 0.05$ by the paired Student *t*-test was considered significant.

3. Results and discussion

ROS production of healthy or CGD neutrophils upon stimulation with PMA was detected by chemiluminescence. The production of both $^1O_2$ and $O_2^{\cdot-}$ of healthy neutrophils was observed. The administration of edaravone (10 μM) or PBN (4 mM), a scavenger of singlet oxygen [9,10], suppressed $^1O_2$, but not $O_2^{\cdot-}$ production (Fig. 1A). Neither $^1O_2$ nor $O_2^{\cdot-}$ release from CGD neutrophils was observed (Fig. 1B).

NET formation by PMA was visualized by fluorescence microscopy and SEM. NET formation was observed at 3 h after PMA stimulation in healthy neutrophils. The treatment of $^1O_2$ scavenger, edaravone (10 μM) or PBN (4 mM) significantly suppressed NET formation by fluorescence microscopy (Fig. 2A, upper panel) and by SEM (Fig. 2A, lower panel). Quantitative analysis was performed using ImageJ software (Fig. 2A, right graph). In contrast, CGD neutrophils did not exhibit NET formation (Fig. 2B), which is consistent

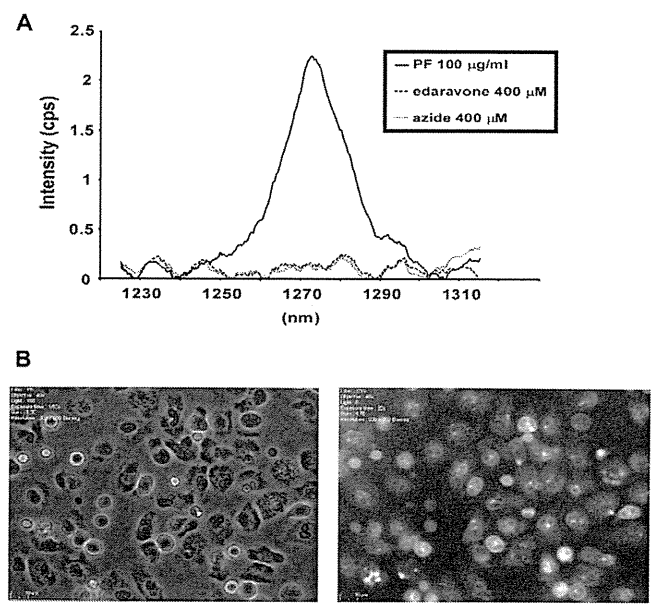

Fig. 3. $^1O_2$ generation by Photofrin in a cell-free system and accumulation of Photofrin in neutrophils. (A) Detection of $^1O_2$ by near-infrared luminescence in a cell-free system. The direct analysis of near-infrared luminescence was performed using Raman spectroscopy, to detect $^1O_2$, which was generated by porfimer sodium (Photofrin (PF), 100 μg/ml) with irradiation using a laser beam (λ = 632.8 nm, power 6 mW) in D_2O solution. The quantum yields of $^1O_2$ production were determined by measurements of the $^1O_2$ luminescence at 1270 nm. The scavenging activity for $^1O_2$ of edaravone (400 μM) or azide (400 μM) was observed. (B) Accumulation of Photofrin in neutrophils. Subcellular localization of Photofrin (10 μg/ml) in neutrophils (2×10^7 cells/ml) was determined by fluorescent microscopy (400×). The phase contrast image (left panel) and the fluorescence image for Photofrin (right panel) are shown. Note that Photofrin was accumulated in the cytosol of neutrophils.

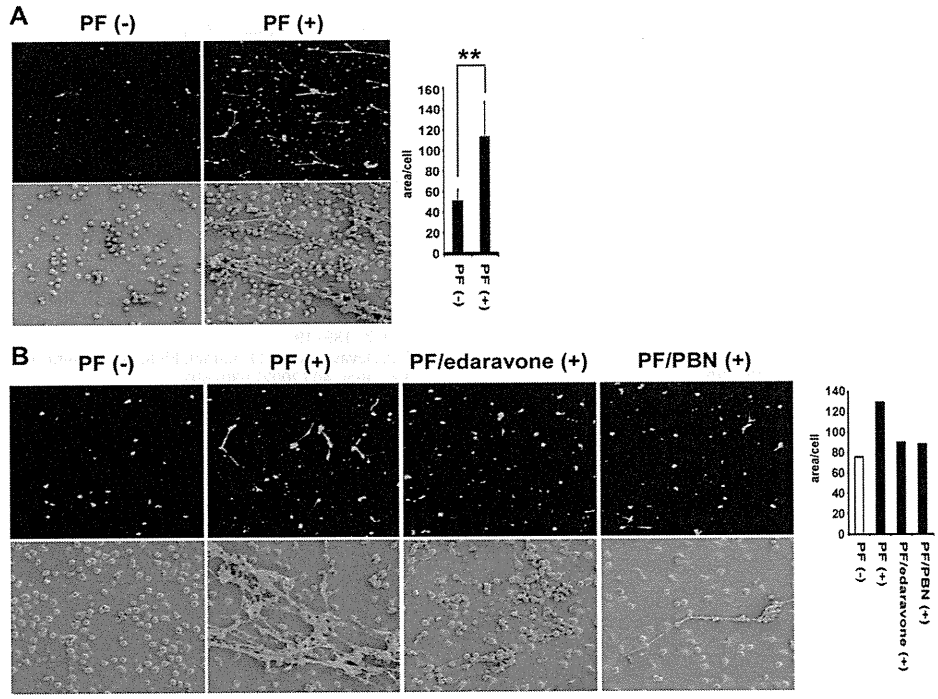

Fig. 4. NET formation of healthy or CGD neutrophils by $^1O_2$-generating system with Photofrin/irradiation. (A) NET formation of healthy neutrophils in the treatment with Photofrin/irradiation by fluorescence confocal microscopy (upper panels, 100×) and SEM (lower panels, 250×). Representative data are shown. Quantitative analysis was performed (right graph). NET formation was observed at 1 h after the treatment with 10 μg/ml Photofrin and 5 min irradiation using an LED lamp (λ_{max} = 660 nm). Values are the means ± SD (n = 6). ** Indicates $P < 0.01$. (B) NET formation of CGD neutrophils in the treatment with Photofrin/irradiation by fluorescence confocal microscopy (upper panels, 100×) and SEM (lower panels, 250×). CGD neutrophils formed NETs by Photofrin/irradiation treatment. The inhibitory effect of edaravone (10 μM) or PBN (4 mM) on NET formation in the treatment with Photofrin/irradiation was observed. Quantitative analysis was also performed (right graph).

with previous reports [4,13]. A recent study showed that myeloperoxidase (MPO) is required for NET formation [8]. It is difficult to identify which ROS is essential for NET formation, since some ROS, such as $^1O_2$ and HOCl, are generated downstream of MPO. We previously reported that edaravone was a $^1O_2$ scavenger [9], but it has been reported that edaravone quenches HOCl and hydroxyl radical as well [14]. In the current study, we used another $^1O_2$ scavenger, PBN, which neither affects MPO activity, nor reacts with HOCl [10]. PBN significantly suppressed NET formation (Fig. 2A), suggesting that $^1O_2$ is involved in NET formation.

We next explored the direct effect of $^1O_2$ in NET formation. First, we examined $^1O_2$ generation by the most specific method, using Photofrin (PF) in a cell-free system [15], which was detected by direct analysis of near-infrared luminescence at 1270 nm (Fig. 3A). It was found that 400 μM edaravone almost completely suppressed the $^1O_2$ spectrum, as well as 400 μM azide, a well-known $^1O_2$ scavenger (Fig. 3A). These findings indicated that $^1O_2$ was generated in this system using Photofrin with light irradiation, and further supported that edaravone is a direct $^1O_2$ scavenger. The accumulation of Photofrin in neutrophils was observed by fluorescence confocal microscopy (Fig. 3B), indicating that $^1O_2$ was generated in neutrophils by Photofrin with light irradiation.

NET formation by Photofrin/irradiation was visualized by fluorescence microscopy and SEM. NET formation was observed in healthy neutrophils (Fig. 4A). Quantitative analysis was performed using ImageJ software (Fig. 4A, right graph). Interestingly, CGD neutrophils made NETs by Photofrin/irradiation as well (Fig. 4B). It is noteworthy that CGD neutrophils did not exhibit NET formation by PMA stimulation, which is dependent on Nox activation (Fig. 2B). This was suppressed by $^1O_2$ scavengers, edaravone (10 μM) or PBN (4 mM) (Fig. 4B). These results suggested that $^1O_2$ directly induced NET formation in both healthy and CGD neutrophils, independent of Nox activation. The modulation of NET formation should be effective in the control of infectious or inflammatory disorders. From the current study, the suppression of $^1O_2$ could be an optimal target for regulating NET formation, minimalizing impairment of innate host defense.

Author contributions

Y.N., T.A., and K.Y. designed and performed experiments, analyzed the data, and prepared the paper. S.A. and A.T.-K. supervised the study.

Acknowledgments

The authors thank Tomoko Numata, Yasushi Nakata (HORIBA, Ltd.), Keiko Furuta, and Haruyasu Kohda (Division of Electron Microscopic Study, Center for Anatomical Studies, Graduate School of Medicine, Kyoto University) for excellent technical assistance. This work was supported by the Ministry of Education, Science, Sports, and Culture of Japan.

References

[1] V. Brinkmann, U. Reichard, C. Goosmann, B. Fauler, Y. Uhlemann, D.S. Weiss, Y. Weinrauch, A. Zychlinsky, Neutrophil extracellular traps kill bacteria, Science 303 (2004) 1532–1535.

[2] V. Brinkmann, A. Zychlinsky, Beneficial suicide: why neutrophils die to make NETs, Nat. Rev. Microbiol. 5 (2007) 577–582.

[3] C.F. Urban, D. Ermert, M. Schmid, U. Abu-Abed, C. Goosmann, W. Nacken, V. Brinkmann, P.R. Jungblut, A. Zychlinsky, Neutrophil extracellular traps contain calprotectin, a cytosolic protein complex involved in host defense against *Candida albicans*, PLoS Pathog. 5 (2009) e1000639.

[4] T.A. Fuchs, U. Abed, C. Goosmann, R. Hurwitz, I. Schulze, V. Wahn, Y. Weinrauch, V. Brinkmann, A. Zychlinsky, Novel cell death program leads to neutrophil extracellular traps, J. Cell Biol. 176 (2007) 231–241.

[5] S.J. Klebanoff, Myeloperoxidase: friend and foe, J. Leukoc. Biol. 77 (2005) 598–625.

[6] B.M. Babior, C. Takeuchi, J. Ruedi, A. Gutierrez, P. Wentworth Jr., Investigating antibody-catalyzed ozone generation by human neutrophils, Proc. Natl. Acad. Sci. USA 100 (2003) 5130–5135.

[7] K. Yamashita, T. Miyoshi, T. Arai, N. Endo, H. Itoh, K. Makino, K. Mizugishi, T. Uchiyama, M. Sasada, Ozone production by amino acids contributes to killing of bacteria, Proc. Natl. Acad. Sci. USA 105 (2008) 16912–16917.

[8] K.D. Metzler, T.A. Fuchs, W.M. Nauseef, D. Reumaux, J. Roesler, I. Schulze, V. Wahn, V. Papayannopoulos, A. Zychlinsky, Myeloperoxidase is required for neutrophil extracellular trap formation: implications for innate immunity, Blood 117 (2011) 953–959.

[9] P. Sommani, T. Arai, K. Yamashita, T. Miyoshi, H. Mori, M. Sasada, K. Makino, Effects of edaravone on singlet oxygen released from activated human neutrophils, J. Pharmacol. Sci. 103 (2007) 117–120.

[10] A. Kawai, Y. Nishinaka, T. Arai, K. Hirota, H. Mori, N. Endo, T. Miyoshi, K. Yamashita, M. Sasada, Alpha-phenyl-N-tert-butyl nitrone has scavenging activity against singlet oxygen ((1)O(2)) and attenuates (1)O(2)-induced neuronal cell death, J. Pharmacol. Sci. 108 (2008) 545–549.

[11] G.H. Posner, J.R. Lever, K. Miura, C. Lisek, H.H. Seliger, A. Thompson, A chemiluminescent probe specific for singlet oxygen, Biochem. Biophys. Res. Commun. 123 (1984) 869–873.

[12] M. Nakano, K. Sugioka, Y. Ushijima, T. Goto, Chemiluminescence probe with Cypridina luciferin analog, 2-methyl-6-phenyl-3,7-dihydroimidazo[1,2-α]pyrazin-3-one, for estimating the ability of human granulocytes to generate O_2, Anal. Biochem. 159 (1986) 363–369.

[13] M. Bianchi, A. Hakkim, V. Brinkmann, U. Siler, R.A. Seger, A. Zychlinsky, J. Reichenbach, Restoration of NET formation by gene therapy in CGD controls aspergillosis, Blood 114 (2009) 2619–2622.

[14] K. Sumitomo, N. Shishido, H. Aizawa, N. Hasebe, K. Kikuchi, M. Nakamura, Effects of MCI-186 upon neutrophil-derived active oxygens, Redox Rep. 12 (2007) 189–194.

[15] T.P. Devasagayam, J.P. Kamat, Biological significance of singlet oxygen, Indian J. Exp. Biol. 40 (2002) 680–692.

blood

2011 117: 500-509
Prepublished online October 18, 2010;
doi:10.1182/blood-2010-05-284737

Bortezomib suppresses function and survival of plasmacytoid dendritic cells by targeting intracellular trafficking of Toll-like receptors and endoplasmic reticulum homeostasis

Makiko Hirai, Norimitsu Kadowaki, Toshio Kitawaki, Haruyuki Fujita, Akifumi Takaori-Kondo, Ryutaro Fukui, Kensuke Miyake, Takahiro Maeda, Shimeru Kamihira, Yoshiki Miyachi and Takashi Uchiyama

Blood (print ISSN 0006-4971, online ISSN 1528-0020), is published weekly by the American Society of Hematology, 2021 L St, NW, Suite 900, Washington DC 20036.

Bortezomib suppresses function and survival of plasmacytoid dendritic cells by targeting intracellular trafficking of Toll-like receptors and endoplasmic reticulum homeostasis

Makiko Hirai,[1] Norimitsu Kadowaki,[2,3] Toshio Kitawaki,[2] Haruyuki Fujita,[2] Akifumi Takaori-Kondo,[2] Ryutaro Fukui,[4] Kensuke Miyake,[4] Takahiro Maeda,[5] Shimeru Kamihira,[6] Yoshiki Miyachi,[1] and Takashi Uchiyama[2,7]

Departments of [1]Dermatology and [2]Hematology and Oncology, Graduate School of Medicine, Kyoto University, Kyoto, Japan; [3]Japan Science and Technology Agency, Core Research for Evolutional Science and Technology (CREST), Tokyo, Japan; [4]Division of Infectious Genetics, The Institute of Medical Science, The University of Tokyo, Tokyo, Japan; Departments of [5]Island and Community Medicine and [6]Laboratory Medicine, Nagasaki University Graduate School of Biomedical Sciences, Nagasaki, Japan; and [7]Kitano Hospital, The Tazuke Kofukai Medical Research Institute, Osaka, Japan

Dendritic cells (DCs) play a pivotal role in the pathogenesis of inflammatory disorders, so suppressing the activity of DCs is instrumental in treating such diseases. In the present study, we show that a proteasome inhibitor, bortezomib, suppresses the survival and immunostimulatory function of human plasmacytoid DCs (pDCs) by targeting 2 critical points, intracellular trafficking of nucleic acid-sensing Toll-like receptors (TLRs) and endoplasmic reticulum (ER) homeostasis. Among the immune cells in blood, pDCs were the most susceptible to the killing effect of bortezomib. This correlates with a decrease in the spliced form of a transcription factor XBP1, which rescues cells from apoptosis by maintaining ER homeostasis. Bortezomib suppressed the production of interferon-α and interleukin-6 by pDCs activated with a TLR9-stimulating CpG DNA and a TLR7-stimulating influenza virus, which appears to be partially independent of apoptosis. Bortezomib inhibited translocation of TLR9 from the ER to endolysosomes but not of an ER membrane protein, Unc93B1, that delivers TLR9 to endolysosomes. Thus, bortezomib suppresses the activity of pDCs by inhibiting intracellular trafficking of TLRs through disrupting the coordinated translocation of TLRs and Unc93B1 and by disturbing ER homeostasis. This study suggests that proteasome inhibitors may alleviate inflammatory disorders such as lupus and psoriasis that involve pDCs. (*Blood.* 2011;117(2):500-509)

Introduction

Dendritic cells (DCs) play a pivotal role in controlling immune responses by linking innate and adaptive arms of the immune system.[1] Thus, DCs represent an important target for the treatment of a variety of immune-related disorders.

In humans, DCs are composed of 2 subsets: plasmacytoid DCs (pDCs) and myeloid DCs (mDCs).[2] These DCs express different sets of nucleic acid-sensing Toll-like receptors (TLRs): pDCs express TLR7 and TLR9, whereas mDCs express TLR3 and TLR8.[3] pDCs are distinguished from other immune cells by their remarkable potency to produce interferon (IFN)-α in response to virus-derived single-stranded RNA or CpG DNA though TLR7 or TLR9, respectively.[4] Because of this distinctive capacity, it has been assumed that pDCs play an important role in antiviral immune responses.[5] On the other hand, it has been shown that if the nucleic acids are derived from self tissues, pDCs cause inflammatory disorders such as systemic lupus erythematosus (SLE) and psoriasis.[6] In SLE, immune complexes containing self DNA or RNA are incorporated into pDCs and induce them to produce IFN-α via TLR9[7,8] or TLR7,[8,9] respectively. It is proposed that such IFN-α production plays a key role in the pathogenesis of SLE.[10,11] In psoriasis, aggregated particles composed of self DNA and RNA from damaged epithelial cells and the antimicrobial peptide LL37 are incorporated into pDCs and induce them to produce IFN-α via TLR9[12] and TLR7,[13] respectively, thus contributing to the pathogenesis. Therefore, suppressing IFN-α production by pDCs may represent a novel therapy for these inflammatory disorders in which pDCs are likely to play an important role.

A recent study has suggested that maintenance of endoplasmic reticulum (ER) homeostasis by the transcription factor XBP1 is essential for the development and survival of pDCs, thus representing a possible target for controlling their activity.[14] Proper functioning of highly secretory cells such as pDCs depends on the unfolded protein response (UPR), that is, coordinated handling of ER stress caused by a burden of unfolded proteins in the lumen of the ER.[15] After sensing unfolded proteins, an ER-resident transmembrane endoribonuclease, IRE1, exhibits unconventional splicing activity on XBP1 mRNA, which results in the conversion of an inactive, unspliced XBP1 (XBP1u) to an active, spliced XBP1 (XBP1s) protein. XBP1s induces the transcription of a broad array of UPR genes that assist in protein synthesis and secretion.[16,17] Development of XBP1-deficient pDCs is reduced, likely due to their increased sensitivity to apoptosis induced by ER stress.[14]

Another important step for the physiologic activity of pDCs is intracellular trafficking of nucleic acid-sensing TLRs from the ER

Submitted May 9, 2010; accepted September 26, 2010. Prepublished online as *Blood* First Edition paper, October 18, 2010; DOI 10.1182/blood-2010-05-284737.

An Inside *Blood* analysis of this article appears at the front of this issue.

The online version of this article contains a data supplement.

An Inside *Blood* analysis of this article appears at the front of this issue.

The publication costs of this article were defrayed in part by page charge payment. Therefore, and solely to indicate this fact, this article is hereby marked "advertisement" in accordance with 18 USC section 1734.

to endolysosomes.[18] Recent studies have revealed that a multiple membrane-spanning protein, Unc93B1, physically interacts with nucleic acid-sensing TLRs (TLR3, TLR7, and TLR9) in the ER and delivers them to endolysosomes, where the TLRs transmit an activating signal.[19,20] Thus, the interaction between nucleic acid-sensing TLRs and Unc93B1 constitutes another target for controlling the activity of pDCs.

A selective inhibitor of the 26S proteasome, bortezomib, has been established as an effective drug for plasma cell myeloma.[21] Although multiple mechanisms have been reported for the antitumor activity of bortezomib,[21] growing evidence suggests that the selectivity of bortezomib for myeloma may be explained by increased susceptibility of myeloma cells to ER stress-induced apoptosis,[22,23] which is consistent with a crucial role of XBP1 in the development of plasma cells[24,25] and in the pathogenesis of myeloma.[26] Bortezomib is likely to disturb ER homeostasis of myeloma cells by targeting several points. For example, proteasome inhibitors have been shown to suppress the activity of IRE1 and to stabilize the dominant-negative XBP1u protein, resulting in a decrease in the activity of XBP1s in myeloma cells.[22] Proteasome inhibitors also prevent retrograde translocation of misfolded proteins in the ER to the cytosol, resulting in the accumulation of a large amount of misfolded immunoglobulin in the ER of myeloma cells.[27] Such overloading of the ER might compromise its physiologic functions. pDCs resemble plasma cells in that both have the developed ER,[28] are highly secretory, and depend on ER homeostasis, particularly on XBP1, for their development and survival.[14,24,25] Furthermore, coordinated trafficking of the 2 ER-resident proteins, TLR and Unc93B1, is necessary for pDCs to respond to the TLR ligands.[20] Therefore, we hypothesized that bortezomib may suppress the activity of pDCs by targeting the 2 critical events in the ER: the UPR and the coordinated function of the ER-resident TLRs and Unc93B1.

In the present study, we investigated the effects of bortezomib on human pDCs. We show that bortezomib inhibits the production of IFN-α by blocking intracellular trafficking of nucleic acid-sensing TLRs at an early stage, and thereafter induces apoptosis of pDCs, which is correlated with the suppression of XBP1 splicing. These results have significant implications for the physiologic mechanisms of survival and activation of pDCs and for the application of proteasome inhibitors to inflammatory disorders in which pDCs play a key role.

Methods

Culture media, reagents, and cell lines

RPMI 1640 (Sigma-Aldrich) supplemented with 10% heat-inactivated fetal calf serum (ThermoTrace), 2mM L-glutamine, penicillin G, streptomycin (Gibco BRL), and 10mM HEPES (N-2-hydroxyethylpiperazine-N′-2-ethanesulfonic acid; Nacalai Tesque) was used for cell culture. Bortezomib, which was provided by Millennium Pharmaceuticals, was dissolved in dimethylsulfoxide at 10mM as a stock solution and was stored at −20°C. Influenza virus ($10^{5.3}$ median tissue culture infective dose/0.2 mL of A/Niigata/05F254/2006), a kind gift from Dr Reiko Saito (Niigata University, Niigata, Japan), was inactivated at 56°C for 30 minutes and added at 0.1% vol/vol to the cell culture. A cell line derived from blastic plasmacytoid dendritic cell neoplasm CAL-1 was described previously by Maeda et al.[29] The myeloma cell line RPMI 8226 was obtained from ATCC.

Isolation of pDCs

This study was approved by the Institutional Review Board of the Graduate School of Medicine at Kyoto University and abides by the tenets of the Declaration of Helsinki. Peripheral blood mononuclear cells (PBMCs) were obtained from healthy donors with written informed consent in accordance with the Declaration of Helsinki. pDCs were isolated as described in Kawamura et al.[30] In brief, $CD4^+CD11c^-lin^-$ cells were isolated as pDCs using an FACSAria cell sorter (BD Biosciences). Reanalysis of the sorted cells confirmed a purity of more than 98%.

Cell viability assays

PBMCs (2×10^6 cells/2 mL in 12-well culture plates) were cultured with bortezomib for 6 or 24 hours. The cells were stained with the following combinations of monoclonal antibodies (mAbs): fluorescein isothiocyanate (FITC)–conjugated anti-CD3 (BD Biosciences) and PE-conjugated anti-CD56 mAbs (Beckman Coulter); FITC-conjugated CD19 (BD Biosciences) and PE-conjugated anti-BDCA-1 mAbs (Miltenyi Biotec); or FITC-conjugated anti-BDCA-2 (Miltenyi Biotec) and PE-conjugated anti-CD14 mAbs (Beckman Coulter). T cells ($CD3^+$), natural killer (NK) cells ($CD3^-CD56^+$), B cells ($CD19^+$), mDCs ($BDCA\text{-}1^+CD19^-$), pDCs ($BDCA\text{-}2^+$), and monocytes ($CD14^+$) were identified by flow cytometry using the FACSCalibur (BD Biosciences). Dead cells were excluded by staining with propidium iodide. Viable cell numbers of each cell population were counted using Flow-Count Fluorospheres (Beckman Coulter) according to the manufacturer's instructions. Purified pDCs (4×10^4 cells/200 μL in round-bottom, 96-well culture plates) were cultured with bortezomib for 3 hours and stimulated with 0.5μM oligodeoxynucleotide 2216 (ODN2216) (CpG-A)[31] (Operon Biotechnologies) in the presence of bortezomib for 24 hours. The cells were stained with FITC-conjugated CELL LAB ApoScreen annexin V (Beckman Coulter) and propidium iodide and were analyzed for viability by flow cytometry with the FACSCalibur. Alternatively, pDCs were treated with the pan-caspase inhibitor benzyloxycarbonyl-V-A-D-O-methyl fluoromethyl ketone (50μM Z-VAD-FMK; R&D Systems) together with bortezomib and 0.5μM ODN2216, stained with FITC-conjugated annexin V, and analyzed by flow cytometry. The percentages of specific death induced by bortezomib were calculated as 100 × (experimental death % − spontaneous death %)/(100 − spontaneous death %), in which the percentages of experimental or spontaneous death were defined as the percentages of annexin V–positive cells in the presence or absence of bortezomib, respectively.

RT and real-time PCR

Cells were treated with tunicamycin (Wako Pure Chemical Industries) at 0.4 μg/mL for CAL-1, 0.8 μg/mL for RPMI 8226, or 5 μg/mL for pDCs and T cells to induce ER stress. Total RNA was isolated using the QIAshredder and RNeasy Mini Kit (QIAGEN). First-strand cDNA synthesis was performed with the ReverTra Ace qPCR RT kit (Toyobo). Real-time polymerase chain reaction (PCR) was performed on the Thermal Cycler Dice real-time system (TaKaRa). XBP1 was detected using SYBR Premix Ex Taq (TakaRa) and gene-specific oligonucleotide primers as follows: for the *XBP1u* gene: 5′-CGAATGAGTGAGCTGGAACA-3′ (forward) and 5′-CTGCAGAGGTGCACGTAGTC-3′ (reverse); for the *XBP1s* gene: 5′-CGAATGAGTGAGCTGGAACA-3′ (forward) and 5′-CTGCACCTGCTGCGGACT-3′ (reverse).

IFN-α1 and β-glucuronidase (GUS) were detected using TaqMan gene expression assays (Applied Biosystems) and the THUNDERBIRD Probe qPCR mix (Toyobo). Relative quantitation of mRNA expression was performed using the ΔΔCt method. The mRNA expression levels of each gene were normalized to those of GUS.

Analysis of cytokine production by ELISA

Cytokines in the supernatants were analyzed by enzyme-linked immunosorbent assay (ELISA). The following reagents were used: the human IFN-α module set (Bender MedSystems) and the human interleukin-6 (IL-6) ELISA MAX Standard set (BioLegend).

Retroviral transduction

HEK293T cells were cotransfected with retroviral vectors (pMXpuro carrying a green fluorescent protein [GFP])–tagged mouse *TLR9* gene[32] or

pMXneo carrying a GFP-tagged mouse *UNC93B1* gene[33]) and retroviral packaging plasmids (pMLVg/p and pVSV-G) using the CalPhos mammalian transfection kit (Clontech). Forty-eight hours after transfection, the supernatant was collected. The mouse B-cell line M12[32] was infected with the virus suspension.

Confocal analysis of intracellular trafficking of TLR9 and Unc93B1

M12 cells expressing TLR9-GFP or Unc93B1-GFP were cultured in the absence or presence of 30nM bortezomib for 1 hour, and stimulated with 0.5μM ODN1668[34] (Operon Biotechnologies) in the absence or presence of 30nM bortezomib for 2 hours. ER-Tracker Red or LysoTracker Red DND-99 (Invitrogen) was added for 30 minutes before the harvest. After fixation with 4% paraformaldehyde for 15 minutes at 37°C, the cells were attached to poly-L-lysine–coated slides and examined with a laser scanning 510 confocal microscope with an αPlan-Fluar 100×/1.45 numeric aperture oil-immersion objective (Carl Zeiss). Data were acquired with the laser scanning microscope software (LSM 510, Version 3.2 SP2 software; Carl Zeiss).

Confocal analysis of nuclear translocation of IRF-7 and NF-κB

Purified pDCs were cultured in the absence or presence of 10nM bortezomib for 3 hours, and were stimulated with 0.5μM ODN2216 in the absence or presence of 10nM bortezomib for 3 hours. After fixation with 2% paraformaldehyde for 15 minutes at 37°C and permeabilization with 100% methanol for 10 minutes at −20°C, the cells were stained with rabbit anti–IFN regulatory factor 7 (anti–IRF-7) or nuclear factor κB (NF-κB) p65 polyclonal antibody (Santa Cruz Biotechnology) and with Alexa Fluor 488-conjugated goat anti–rabbit immunoglobulin G (Invitrogen) as a secondary antibody. Nuclei were identified using TOTO-3 dye (Invitrogen). The cells were attached to slides using a Cytospin centrifuge and examined by confocal microscopy.

Statistical analysis

Data are presented as means ± standard error (SE). Statistical comparisons were performed using paired one-tailed *t* tests, with a P value $< .05$ taken to indicate significance.

Results

pDCs are most susceptible to the killing effect of bortezomib among immune cells in blood

We first examined the viability of each mononuclear cell population in the peripheral blood after culture with bortezomib alone. PBMCs were cultured with bortezomib for 6 hours, washed to remove bortezomib, and then cultured for 18 hours. Alternatively, PBMCs were cultured with bortezomib for 24 hours. Thereafter, the viability of each mononuclear cell population was examined by staining the cells with fluorochrome-conjugated mAbs ($CD3^+$ for T cells, $CD3^-CD56^+$ for NK cells, $CD19^+$ for B cells, $CD14^+$ for monocytes, BDCA-1^+CD19^- for mDCs, and BDCA-2^+ for pDCs) and propidium iodide. Bortezomib was added at 3-100nM (1.15-38.5 ng/mL), which are the clinically relevant concentrations observed in blood after administration.[35,36] The 6-hour exposure to bortezomib mimics the situation in which concentrations are transiently elevated after administration. Resting T cells were the most resistant to the killing effect of bortezomib (Figure 1A), which is consistent with a previous report by Blanco et al.[37] NK cells, B cells, and monocytes are more susceptible to the killing effect than are T cells. Bortezomib killed mDCs more than these cells. Notably, pDCs were the most susceptible to the killing effect, and even short-term exposure to 10nM bortezomib greatly reduced their viability after 24 hours.

We further examined whether bortezomib also reduces the viability of pDCs stimulated with the TLR9 ligand ODN2216 (CpG-A). Because pDCs cannot be unequivocally identified among PBMCs after stimulation with CpG ODN due to the change of their surface phenotype,[38] we purified pDCs, stimulated them with ODN2216 in the absence or presence of different concentrations of bortezomib for 24 hours, and analyzed their viability with annexin V and propidium iodide staining (Figure 1B). Whereas the majority of pDCs underwent apoptosis without stimulation, as shown in previous studies,[28,39] stimulation with ODN2216 greatly improved the viability. A bortezomib concentration of 30nM or above strongly induced apoptosis of ODN2216-stimulated pDCs.

These data indicate that, among the different populations of PBMCs, bortezomib has the strongest killing effect on pDCs in a resting condition and also induces apoptosis of pDCs stimulated with CpG ODN.

Inhibition of XBP1 splicing correlates with the induction of apoptosis of pDCs by bortezomib

Because it has been shown that XBP1 is essential for the development of plasma cells[24,25] and pDCs,[14] and that bortezomib disrupts the UPR by inhibiting the generation of spliced XBP1 (XBP1s), the active form of XBP1, in plasma cells,[22] we examined whether bortezomib also inhibits the generation of XBP1s mRNA in pDCs. We cultured primary pDCs, a cell line derived from blastic plasmacytoid dendritic cell neoplasm CAL-1,[29] a myeloma cell line RPMI 8226, and T cells in the absence or presence of bortezomib and tunicamycin, an inhibitor of N-linked glycosylation known to induce ER stress and the UPR. The amounts of XBP1s mRNA and XBP1u mRNA were quantitated by real-time reverse transcription (RT)–PCR, and the ratios of XBP1s to XBP1u were calculated (Figure 2). The addition of tunicamycin increased the amounts of XBP1s mRNA relative to those of XBP1u mRNA in all of the cell types. The addition of bortezomib suppressed the generation of XBP1s mRNA induced by tunicamycin in pDCs, CAL-1, and RPMI 8226, whereas bortezomib did not decrease XBP1s mRNA in T cells, which are resistant to the killing effect of bortezomib (Figure 1A). Thus, apoptosis of pDCs is correlated with the decrease in XBP1s, suggesting that disruption of ER homeostasis by bortezomib results in apoptosis of pDCs as well as of plasma cells.[22]

Bortezomib suppresses cytokine production by pDCs stimulated with CpG ODN or influenza virus

Next we examined whether bortezomib suppresses cytokine production by pDCs stimulated with ODN2216 (a TLR9 ligand) or influenza virus (a TLR7 ligand). We pretreated PBMCs with different concentrations of bortezomib for 6 hours, washed the cells to remove bortezomib, and cultured them with the TLR ligands for 24 hours. Alternatively, we pretreated PBMCs with bortezomib for 6 hours, added the TLR ligands without removing bortezomib, and cultured the cells for 24 hours. The concentrations of IFN-α in the supernatants were then measured by ELISA. Because the absolute concentrations were variable depending on the donors, the levels of cytokine concentrations were normalized to the maximum value obtained in the absence of bortezomib. Pretreatment with bortezomib suppressed the production of IFN-α induced by ODN2216 or influenza virus in a dose-dependent manner (Figure 3A, Wash [+]). The addition of bortezomib during

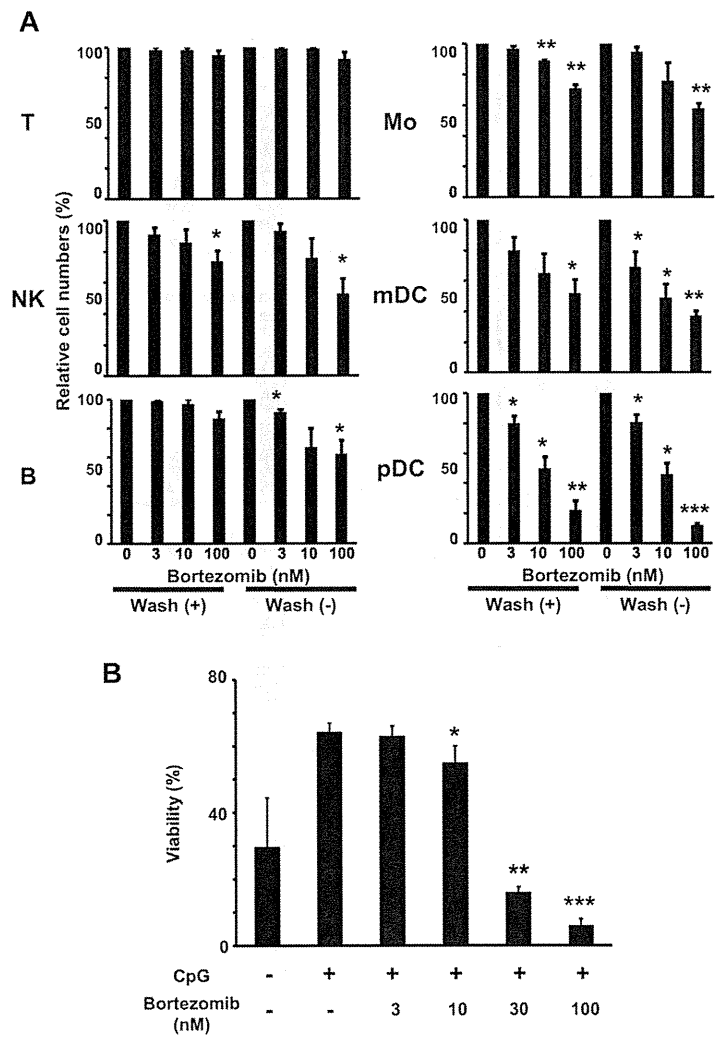

Figure 1. pDCs are susceptible to the killing effect of bortezomib. (A) PBMCs (2×10^6 cells/2 mL) were cultured without or with the indicated concentrations of bortezomib for 6 hours and washed to remove bortezomib. The cell concentration was then adjusted to 1×10^6/mL and further cultured for 18 hours without bortezomib (Wash [+]). Alternatively, PBMCs (2×10^6 cells/2 mL) were cultured without or with bortezomib for 24 hours (Wash [−]). After staining the PBMCs with mAbs to identify each cell population and with propidium iodide to exclude dead cells, viable cell numbers were counted using Flow-Count Fluorospheres by flow cytometry. Cell numbers in the presence of bortezomib relative to those in the absence of bortezomib were expressed as a percentage. Mo indicates monocytes. (B) Purified pDCs (4×10^4 cells/200 μL) were cultured without or with the indicated concentrations of bortezomib for 3 hours, and stimulated with 0.5μM ODN2216 in the presence of bortezomib for 24 hours. The cells were stained with annexin V and propidium iodide and analyzed by flow cytometry. The numbers indicate the percentages of annexin V and propidium iodide double-negative viable cells. $^*P < .05$; $^{**}P < .01$; $^{***}P < .001$. The data are shown as means ± SE of 3 independent experiments. *P* values refer to the comparison between the data obtained without bortezomib and those obtained with each concentration of bortezomib.

the whole period of culture further suppressed the production of IFN-α (Figure 3A, Wash [−]). These data indicate that bortezomib strongly suppresses the production of IFN-α by pDCs stimulated with the TLR9 or TLR7 ligand in a dose- and time-dependent manner.

We also examined the effect of bortezomib on the production of IFN-α and IL-6 by purified pDCs stimulated with ODN2216. We pretreated purified pDCs with different concentrations of bortezomib for 3 hours, added ODN2216 without removing bortezomib, and cultured the cells for 24 hours. The concentrations of IFN-α and IL-6 in the supernatants were then measured by ELISA. Bortezomib suppressed the production of both IFN-α and IL-6 by purified pDCs in a dose-dependent manner (Figure 3B).

To examine whether the suppression of cytokine production is due to the induction of apoptosis, we stimulated pDCs with ODN2216 in the absence or presence of bortezomib for 4 hours. Viability was then measured with annexin V/propidium iodide staining, and the amounts of IFN-α mRNA were measured by real-time RT-PCR. Whereas viability did not decrease during the culture, bortezomib strongly suppressed the transcription of IFN-α mRNA (Figure 4A). We also cultured pDCs with ODN2216 and different concentrations of bortezomib in the absence or presence of the pan-caspase inhibitor Z-VAD-FMK. The percentages of apoptosis specifically induced by bortezomib were then calculated and the concentrations of IFN-α in the supernatants measured by ELISA. Although Z-VAD-FMK significantly suppressed apoptosis of pDCs induced by each concentration (3, 10, 100nM) of bortezomib, the recovery of IFN-α production by Z-VAD-FMK was marginal and was significant only at 10nM bortezomib (Figure 4B). Based on these data, we concluded that bortezomib suppresses IFN-α production by pDCs in a partly apoptosis-independent manner.

Bortezomib inhibits trafficking of TLR9 but not of Unc93B1 from the ER to endolysosomes induced by CpG ODN

We investigated the mechanisms by which bortezomib suppresses cytokine production by pDCs. The earliest event leading to CpG ODN-induced IFN-α production was endocytosis of CpG ODN by pDCs. Thus, we examined whether bortezomib inhibits uptake of CpG ODN by pDCs. We pretreated pDCs with bortezomib for 3 hours, and then added FITC-conjugated ODN2216. After 90 minutes, we examined the intracellular localization of ODN2216 by confocal microscopy (supplemental Figure 1, available on the *Blood* Web site; see the Supplemental Materials link at the top of the online article). Whereas pDCs kept on ice did not endocytose ODN2216, pDCs cultured at 37°C did. Bortezomib did not inhibit

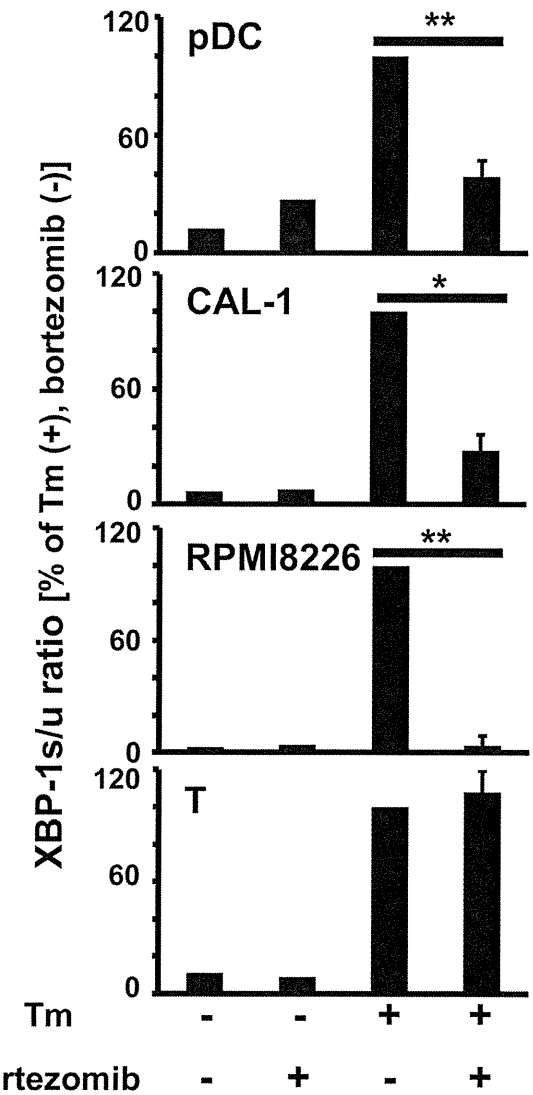

Figure 2. Bortezomib inhibits XBP1 splicing in pDCs. Purified pDCs, the pDC tumor cell line CAL-1, the myeloma cell line RPMI 8226, or resting T cells were cultured without or with 100nM bortezomib for 1 hour, and 5 μg/mL tunicamycin (Tm) was added 4 hours before harvest. The expression levels of XBP1u and XBP1s mRNA were measured by real-time RT-PCR and normalized to those of GUS. The XBP1s/XBP1u ratios were calculated. The data are normalized to the value obtained with tunicamycin in the absence of bortezomib. $*P < .05$; $**P < .01$. The data are shown as means ± SE of 3 (pDC) or 4 (CAL-1, RPMI8226, T) independent experiments.

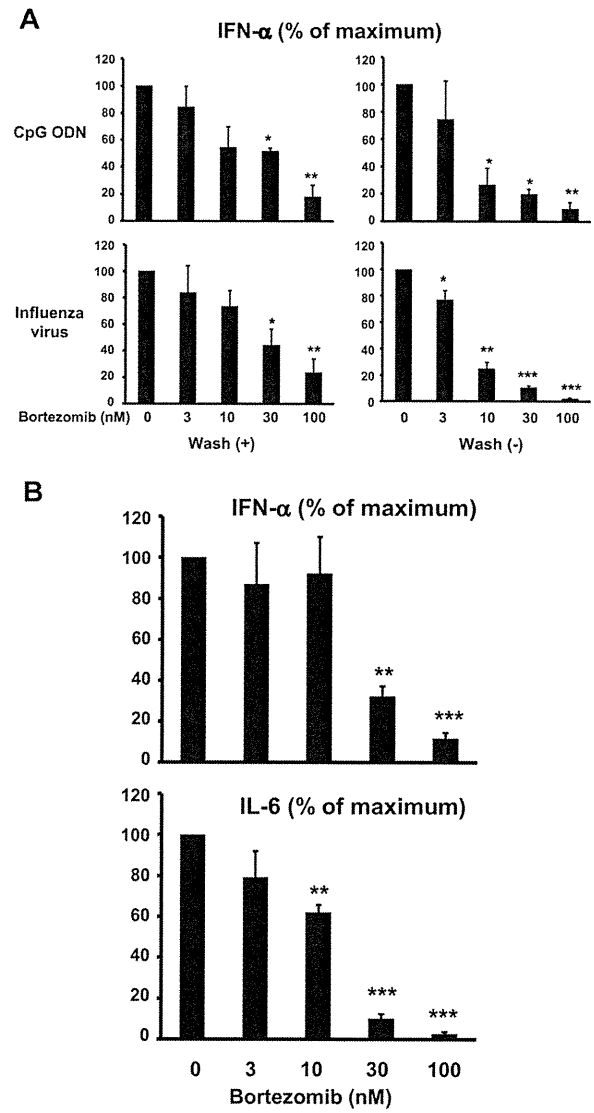

Figure 3. Bortezomib suppresses cytokine production by pDCs stimulated with ODN2216 or influenza virus. (A) PBMCs (1×10^6/mL) were cultured without or with the indicated concentrations of bortezomib for 6 hours and washed to remove bortezomib. The cell concentration was then adjusted to 1×10^6/mL and further cultured for 24 hours in the presence of 0.5μM ODN2216 or influenza virus without bortezomib (Wash [+]). Alternatively, PBMCs (1×10^6/mL) were cultured without or with bortezomib for 6 hours, and cultured for 24 hours in the presence of ODN2216 or influenza virus without removing bortezomib (Wash [−]). Concentrations of IFN-α in the supernatants were measured by ELISA. The data are normalized to the value obtained without bortezomib. $*P < .05$; $**P < .01$; $***P < .001$. The data are shown as means ± SE of 3 independent experiments. *P* values refer to the comparison between the data obtained without bortezomib and those obtained with each concentration of bortezomib. The means and ranges of absolute concentrations are as follows: ODN2216 (Wash [−]) 4292 pg/mL (1674-9455 pg/mL); influenza (Wash [−]) 1278 pg/mL (1008-1538 pg/mL). (B) Purified pDCs (2×10^5/mL) were cultured without or with the indicated concentrations of bortezomib for 3 hours, and cultured for 24 hours in the presence of 0.5μM ODN2216 without removing bortezomib. Concentrations of IFN-α and IL-6 in the supernatants were measured by ELISA. $**P < .01$; $***P < .001$. The data are shown as means ± SE of 3 independent experiments. The means and ranges of absolute concentrations were as follows: IFN-α, 74 312 pg/mL (48 118-92 759 pg/mL); IL-6, 3904 pg/mL (1970-6343 pg/mL).

the endocytosis of ODN2216. Thus, bortezomib targets a signaling pathway(s) farther downstream.

Upon stimulation with CpG ODN, TLR9 rapidly moves from the ER to endolysosomes.[18] Thus, we next examined whether bortezomib inhibits the intracellular trafficking of TLR9. We stimulated the mouse B-cell line M12 expressing TLR9-GFP with ODN1668 in the absence or presence of bortezomib, and examined whether TLR9 colocalizes with an ER marker (ER-Tracker) or a lysosomal marker (LysoTracker) by confocal microscopy. Whereas TLR9 was located in the ER (Figure 5A) but not in the endolysosomes (Figure 5B) without stimulation, TLR9 left the ER (Figure 5A) and moved to the endolysosomes (Figure 5B) after stimulation with CpG ODN. In the presence of bortezomib, TLR9 remained in the ER (Figure 5A) and did not move to endolysosomes (Figure 5B) after stimulation. We also used a human pDC line, CAL-1, and obtained similar results: bortezomib inhibited the trafficking of TLR9 from the ER to endolysosomes induced by ODN2216 (supplemental Figure 2).

Recent studies have revealed that a multiple membrane-spanning protein, Unc93B1, physically interacts with nucleic

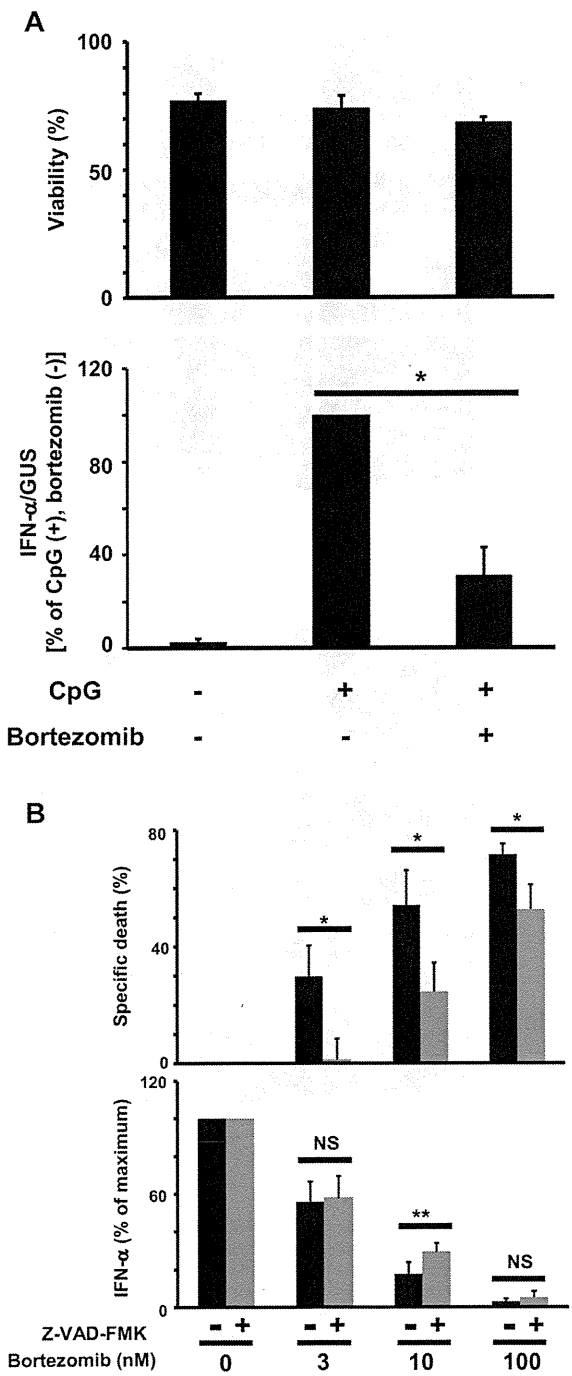

Figure 4. Relationship between viability and IFN-α production by pDCs. (A) Purified pDCs were cultured with 10nM bortezomib for 2 hours and 0.5μM ODN2216 was added. The cells were harvested after 4 hours, stained with FITC-conjugated annexin V, and analyzed for viability by flow cytometry (top panel). IFN-α mRNA was quantitated by real-time RT-PCR, and the expression levels were normalized to those of GUS (bottom panel). The data are normalized to the value obtained with ODN2216 in the absence of bortezomib. $^*P < .05$. The data are shown as means ± SE of 3 independent experiments. (B) After purified pDCs (1×10^5/mL) were cultured without or with 50μM Z-VAD-FMK for 1 hour, the indicated concentrations of bortezomib were added. After 6 hours, 0.5μM ODN2216 was added and the cells and supernatants were harvested 18 hours later. The cells were stained with FITC-conjugated annexin V and analyzed by flow cytometry. The percentages of cell death specifically induced by bortezomib were calculated (top panel). Concentrations of IFN-α in the supernatants were measured by ELISA (bottom panel). The data are normalized to the value obtained without bortezomib. $^*P < .05$; $^{**}P < .01$; NS, not significant. The data are shown as means ± SE of 6 independent experiments.

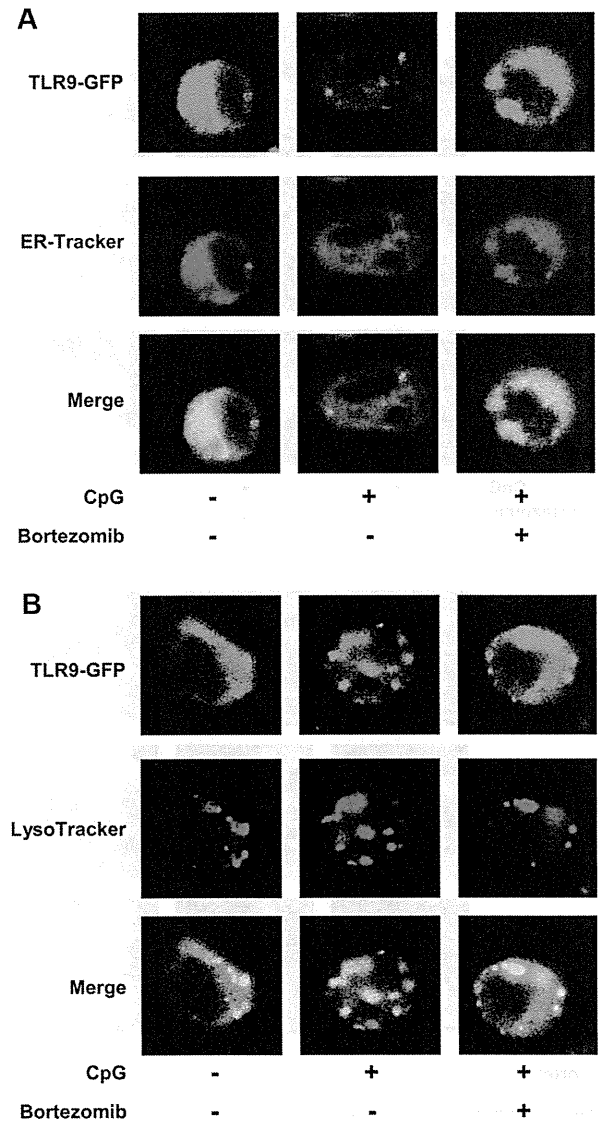

Figure 5. Bortezomib inhibits the trafficking of TLR9 from the ER to endolysosomes induced by CpG ODN. The mouse B-cell line M12 expressing TLR9-GFP was cultured in the absence or presence of 30nM bortezomib for 1 hour and cultured with ODN1668 in the absence or presence of bortezomib for 2 hours. ER-Tracker (A) and LysoTracker (B) were added during the last 30 minutes. The cells were observed by confocal microscopy. The data are representative of 4 experiments.

acid-sensing TLRs in the ER and delivers them to endolysosomes upon stimulation with a TLR ligand.[19,20] Thus, we examined whether bortezomib inhibits the trafficking of TLR9 by inhibiting that of Unc93B1. We stimulated M12 expressing Unc93B1-GFP with ODN1668 in the absence or presence of bortezomib, and examined whether Unc93B1 colocalizes with an ER marker (ER-Tracker) or a lysosomal marker (LysoTracker) by confocal microscopy. Whereas Unc93B1 was located in the ER (Figure 6A) but not in endolysosomes (Figure 6B) without stimulation, Unc93B1 left the ER (Figure 6A) and moved to endolysosomes (Figure 6B) after stimulation with CpG1668. Notably, the translocation of Unc93B1 from the ER to endolysosomes was not abrogated by bortezomib (Figure 6A-B).

These data indicate that bortezomib inhibits the trafficking of TLR9 but not of Unc93B1 from the ER to endolysosomes upon

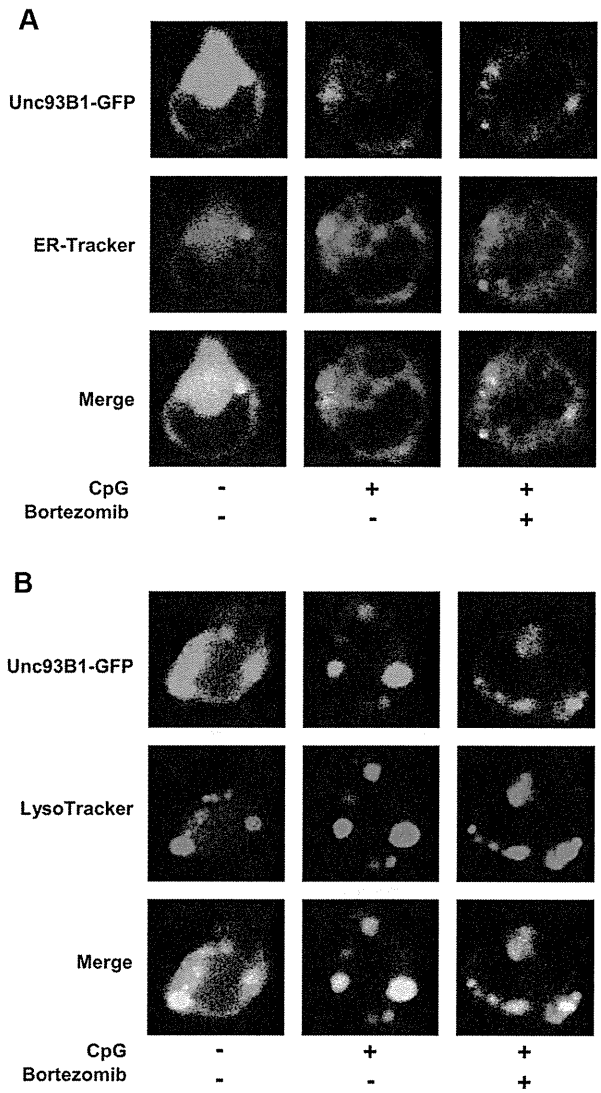

Figure 6. Bortezomib does not inhibit the trafficking of Unc93B1 from the ER to endolysosomes induced by CpG ODN. M12 expressing Unc93B1-GFP was cultured in the absence or presence of 30nM bortezomib for 1 hour and cultured with 0.5μM ODN1668 in the absence or presence of bortezomib for 2 hours. ER-Tracker (A) and LysoTracker (B) were added during the last 30 minutes. The cells were observed by confocal microscopy. The data are representative of 4 experiments.

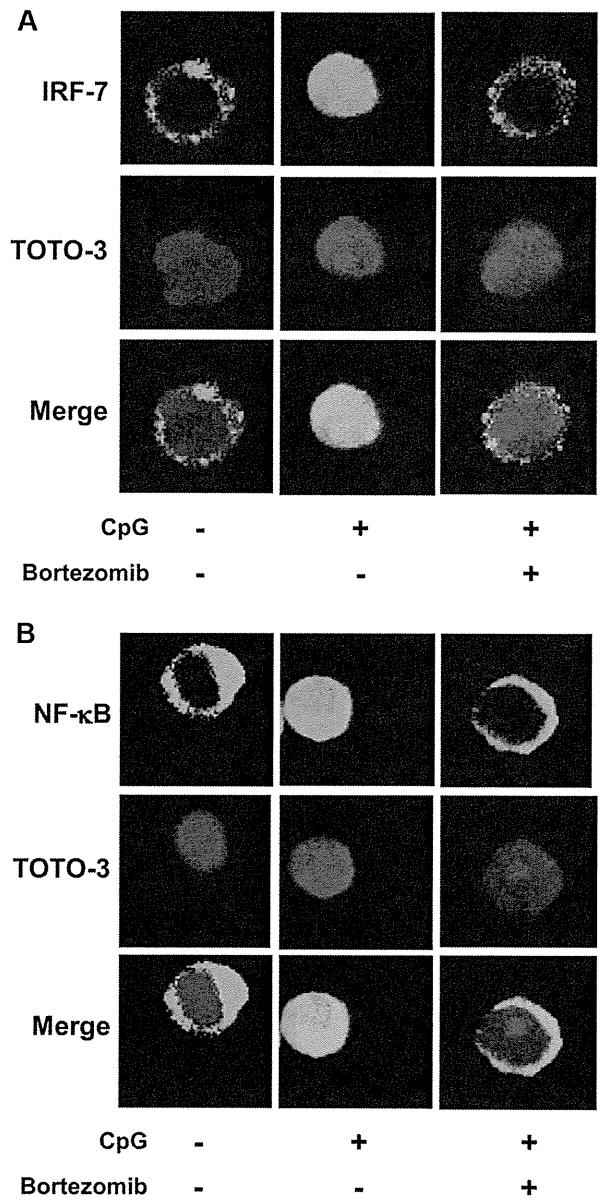

Figure 7. Bortezomib inhibits the nuclear translocation of IRF-7 and NF-κB in pDCs. Purified pDCs were cultured in the absence or presence of 10nM bortezomib for 3 hours and stimulated with 0.5μM ODN2216 for 3 hours. The cells were stained with rabbit anti–IRF-7 (A) or NF-κB p65 (B) and with Alexa Fluor 488–conjugated goat anti–rabbit immunoglobulin G as a secondary antibody. Nuclei were identified using TOTO-3 dye. The data are representative of 3 experiments.

stimulation with CpG ODN. This suggests that bortezomib suppresses the immunostimulatory functions of TLR-triggered pDCs by disrupting the coordinated trafficking of TLR and Unc93B1. In addition, because the inhibition of TLR9 trafficking was observed during the early period of culture (3 hours after adding bortezomib), when apoptosis had not ensued, bortezomib is likely to suppress the immunostimulatory function of pDCs independently of the induction of apoptosis (at least in part).

Bortezomib inhibits nuclear translocation of IRF-7 and NF-κB in pDCs stimulated with CpG ODN

Stimulation of pDCs with CpG ODN induces the nuclear translocation of 2 major transcription factors, IRF-7 and NF-κB, which induce the production of IFN-α and proinflammatory cytokines (TNF-α and IL-6), respectively, at the final step of TLR signaling.[40] Thus, we examined whether bortezomib inhibits the nuclear translocation of IRF-7 and NF-κB induced by ODN2216 in pDCs consistently with the inhibition of intracellular trafficking of TLR9 (Figure 5) and the suppression of IFN-α and IL-6 production (Figure 3). We pretreated pDCs with bortezomib for 3 hours, stimulated them with ODN2216 for 3 hours, and then examined the localization of IRF-7 (Figure 7A) and NF-κB (Figure 7B) by confocal microscopy. Whereas IRF-7 and NF-κB are located in the cytoplasm in untreated pDCs, both of the transcription factors moved to the nucleus after stimulation with ODN2216. Bortezomib inhibited the nuclear translocation of IRF-7 and NF-κB. These data indicate that the inhibition of TLR9 trafficking by bortezomib leads to the abrogation of the nuclear translocation of IRF-7 and NF-κB.

Discussion

Because of the proposed involvement of pDCs in the pathogenesis of several inflammatory disorders, it is of great importance to find reagents that modulate pDC functions. pDCs and plasma cells share a distinctive property, in that both types of cells have a highly developed ER and produce vast amounts of secretory proteins: IFN-α and immunoglobulin, respectively. Therefore, we hypothesized that the proteasome inhibitor bortezomib, which kills myeloma cells partly due to its effect on ER homeostasis, may affect the viability and function of pDCs. The present study had 2 novel findings. First, bortezomib suppresses the immunostimulatory activity of pDCs by disrupting the coordinated translocation of TLR9 and an ER-resident protein, Unc93B1. Second, bortezomib induces apoptosis of pDCs apparently by disturbing ER homeostasis maintained through the activation of XBP1. This is the first study showing the pharmacologic disruption of the coordinated translocation of nucleic acid–sensing TLRs and Unc93B1, and it sheds new light on the molecular mechanisms by which pDCs perform their immune functions and on the mechanisms by which bortezomib executes its immunosuppressive activity.

We first examined the effect of bortezomib on the viability of pDCs using total PBMCs (Figure 1A) or purified pDCs (Figure 1B). Using total PBMCs, we found that of the different immune cell types in blood, pDCs were the most prone to die even after a 6-hour pretreatment with 10nM bortezomib and subsequent culture without bortezomib for 18 hours. Because the majority of purified pDCs spontaneously underwent apoptosis after 24 hours, as shown in previous studies,[28,39] we examined the effect of bortezomib on the viability of purified pDCs (2×10^5/mL) under stimulation with CpG ODN, and found that most of them died after exposure to bortezomib concentrations of 30nM or more. There have been conflicting reports concerning the effect of bortezomib on the viability of pDCs. Kukreja et al reported that the majority of purified pDCs undergo apoptosis after culture either with 100nM bortezomib for 48 hours or with 10nM bortezomib for 24 hours.[41] In contrast, Chauhan et al reported that the majority of 1×10^6 purified pDCs are viable even after culture with 20nM bortezomib for 24 hours.[42] Although the reason for such differences in the viability of pDCs in different studies is not known, it appears that Chauhan et al cultured pDCs at a much higher cell concentration than we did in this study. Such a difference in culture conditions might have resulted in the observed differences in the effect of bortezomib. In any event, our data using total PBMCs and purified pDCs clearly show that pDCs are prone to die after exposure to bortezomib.

Highly secretory cells such as plasma cells[24,25] and exocrine gland acinar cells[43] depend on the UPR for their development and survival, as evidenced in XBP1-deficient conditions. It has been shown that proteasome inhibitors target XBP1 through suppressing the activity of IRE1.[22] pDCs are also highly secretory and depend on XBP1 for their development and survival.[14] Thus, we examined whether bortezomib suppresses the generation of XBP1s in pDCs. We found that bortezomib strongly suppressed XBP1 splicing in bortezomib-susceptible pDCs and in myeloma cells, but not in bortezomib-resistant resting T cells. These data, together with a previous report by Iwakoshi et al,[14] suggest that the suppression of XBP1 splicing by bortezomib leads to the apoptosis of pDCs.

We next examined the effect of bortezomib on the cardinal feature of pDCs: the production of IFN-α in response to TLR7 and TLR9 ligands. We also examined the production of the proinflammatory cytokine IL-6, because IFN-α and IL-6 are induced by different transcription factors (IRF-7[44] and NF-κB,[40] respectively). Bortezomib suppressed the production of IFN-α and IL-6 by pDCs stimulated with the TLR9 ligand ODN2216 (CpG-A), and also the production of IFN-α induced by a TLR7 ligand influenza virus, in a dose-dependent manner. Bortezomib appears to suppress the cytokine production by pDCs independently of the induction of apoptosis, at least in part, because: (1) bortezomib suppressed the trafficking of TLR9 and the induction of IFN-α mRNA at an early time point, when apoptosis of pDCs had not ensued; and (2) a pan-caspase inhibitor, Z-VAD-FMK, rescued the IFN-α production only marginally, whereas the reagent significantly rescued pDCs from apoptosis. However, we cannot exclude the possibility that the diminution of cytokine production reflects early apoptotic signaling. For example, it has been shown that bortezomib induces the generation of reactive oxygen species[45] and the activation of c-Jun NH_2-terminal kinase[46] after ER stress, leading to the mitochondrial apoptotic pathway. Such early apoptotic signals might affect functions of pDCs.

Next we examined the mechanisms by which bortezomib suppresses cytokine production by pDCs. Observation by confocal microscopy showed that bortezomib inhibits the intracellular trafficking of TLR9 from the ER to endolysosomes. Notably, however, bortezomib did not inhibit the trafficking of Unc93B1, which has been reported to deliver nucleic acid-sensing TLRs from the ER to endolysosomes.[20] These data suggest that bortezomib inhibits the responses of pDCs to nucleic acids by disrupting the coordinated movement of TLRs and Unc93B1. We confirmed that such inhibition of the trafficking of TLR9 resulted in the abrogation of nuclear translocation of IRF-7 and NF-κB, which corresponds to the suppression of IFN-α[44] and IL-6[40] production, respectively.

Because the precise molecular mechanisms by which Unc93B1 delivers TLRs from the ER to endolysosomes remain to be determined, the mechanism by which bortezomib disrupts the coordinated trafficking of TLR9 and Unc93B1 is not clear. It is tempting to speculate that the accumulation of misfolded proteins in the ER caused by bortezomib may disturb proper functions of ER-resident proteins responsible for the trafficking of TLR9 and Unc93B1. We have recently shown that wild-type and D34A mutant Unc93B1 preferentially associate and translocate with TLR9 and TLR7, respectively,[33] implying that an ER protein not yet identified interacts with the N-terminal region of Unc93B1 and facilitates the trafficking of Unc93B1-TLR complexes to endolysosomes. Such a mechanism might be disarranged by the overwhelming ER stress caused by bortezomib.

It has been proposed that IFN-α from pDCs stimulated with endogenous nucleic acids plays a key role in the pathogenesis of several autoimmune or inflammatory disorders.[47] First, immune complexes composed of DNA/anti-DNA autoantibodies[7,8] or ribonucleoprotein/anti-ribonucleoprotein autoantibodies[8,9] are incorporated into pDCs and stimulate them to produce IFN-α by triggering TLR9 and TLR7, respectively. Such IFN-α is implicated in the pathogenesis of SLE. Intriguingly, a study using Unc93B1 3d mutant mice, in which Unc93B1 is incapable of binding to TLRs,[20] has shown that nucleic acid–sensing TLRs are required for the optimal production of autoantibodies in lupus-prone strains.[48] Thus, the immune complexes and pDCs appear to constitute a positive feedback loop mediated by the TLR-Unc93B1 interaction. Proteasome inhibitors may disrupt such a vicious cycle by targeting pDCs, resulting in the alleviation of SLE. Second, aggregates composed of the antimicrobial peptide LL37 and self DNA[12] or RNA[13] released from damaged cells are incorporated into pDCs and stimulate them to produce IFN-α by triggering TLR9 and TLR7, respectively, and this IFN-α is implicated in the pathogenesis of psoriasis. Bortezomib may alleviate psoriasis by targeting pDCs. Furthermore, pDCs may be involved in the pathogenesis of